

This is a repository copy of *Importance of Angomonas deanei KAP4 for kDNA arrangement, cell division and maintenance of the host-bacterium relationship*.

White Rose Research Online URL for this paper:  
<https://eprints.whiterose.ac.uk/173214/>

Version: Accepted Version

---

**Article:**

Gonçalves, Camila Silva, Catta-Preta, Carolina Moura Costa, Repolês, Bruno et al. (4 more authors) (Accepted: 2021) Importance of Angomonas deanei KAP4 for kDNA arrangement, cell division and maintenance of the host-bacterium relationship. Scientific Reports. ISSN 2045-2322 (In Press)

---

**Reuse**

Items deposited in White Rose Research Online are protected by copyright, with all rights reserved unless indicated otherwise. They may be downloaded and/or printed for private study, or other acts as permitted by national copyright laws. The publisher or other rights holders may allow further reproduction and re-use of the full text version. This is indicated by the licence information on the White Rose Research Online record for the item.

**Takedown**

If you consider content in White Rose Research Online to be in breach of UK law, please notify us by emailing [eprints@whiterose.ac.uk](mailto:eprints@whiterose.ac.uk) including the URL of the record and the reason for the withdrawal request.

1 **Importance of *Angomonas deanei* KAP4 for kDNA arrangement, cell division and**  
2 **maintenance of the host-bacterium relationship**

3

4 Camila Silva Gonçalves<sup>1,2¶</sup>, Carolina Moura Costa Catta-Preta<sup>3¶</sup>, Bruno Repolês<sup>4</sup>, Jeremy  
5 C. Mottram<sup>3</sup>, Wanderley de Souza<sup>1,2</sup>, Carlos Renato Machado<sup>4\*</sup>, Maria Cristina M.  
6 Motta<sup>1,2\*</sup>

7

8 <sup>1</sup>Laboratório de Ultraestrutura Celular Hertha Meyer, Instituto de Biofísica Carlos Chagas  
9 Filho, Universidade Federal do Rio de Janeiro, 21491-590, Rio de Janeiro, RJ, Brazil.

10

11 <sup>2</sup>Instituto Nacional de Ciência e Tecnologia em Biologia Estrutural e Bioimagem – RJ,  
12 Brazil.

13

14 <sup>3</sup>York Biomedical Research Institute, Department of Biology, University of York,  
15 Wentworth Way, Heslington, York, YO10 5DD, UK.

16

17 <sup>4</sup>Laboratório de Genética Bioquímica, Departamento de Bioquímica e Imunologia,  
18 Instituto de Ciências Biológicas, Universidade Federal de Minas Gerais, Belo Horizonte,  
19 Brazil.

20

21

22

23 ¶Both authors contributed equally to this scientific article

24 \*Corresponding authors: Maria Cristina M. Motta, [motta@biof.ufrj.br](mailto:motta@biof.ufrj.br), Laboratório de  
25 Ultraestrutura Celular Hertha Meyer, IBCCF, CCS, UFRJ, Cidade Universitária, Rio de  
26 Janeiro, CEP 21941-590, Brazil. Carlos Renato Machado, [crmachad@icb.ufmg.br](mailto:crmachad@icb.ufmg.br),  
27 Laboratório de Genética Bioquímica, Departamento de Bioquímica e Imunologia,  
28 Instituto de Ciências Biológicas, Universidade Federal de Minas Gerais, Belo Horizonte,  
29 Brazil.

30

31

32 **Abstract**

33 *Angomonas deanei* coevolves in a mutualistic relationship with a symbiotic bacterium  
34 that divides in synchronicity with other host cell structures. Trypanosomatid  
35 mitochondrial DNA is contained in the kinetoplast and is composed of thousands of  
36 interlocked DNA circles (kDNA). The arrangement of kDNA is related the presence of  
37 histone-like proteins, known as KAPs (kinetoplast-associated proteins), that neutralize  
38 the negatively charged kDNA, thereby affecting the activity of mitochondrial enzymes  
39 involved in replication, transcription and repair. In this study, CRISPR-Cas9 was used to  
40 delete both alleles of the *A. deanei KAP4* gene. Gene-deficient mutants exhibited high  
41 compaction of the kDNA network and displayed atypical phenotypes, such as the  
42 appearance of a filamentous symbionts, cells containing two nuclei and one kinetoplast,  
43 and division blocks. Treatment with cisplatin and UV showed that  $\Delta kap4$  null mutants  
44 were not more sensitive to DNA damage and repair than wild-type cells. Notably, lesions  
45 caused by these genotoxic agents in the mitochondrial DNA could be repaired, suggesting  
46 that the kDNA in the kinetoplast of trypanosomatids has unique repair mechanisms.  
47 Taken together, our data indicate that although KAP4 is not an essential protein, it plays  
48 important roles in kDNA arrangement and replication, as well as in the maintenance of  
49 symbiosis.

50

51 **Key words:** cell division, DNA damage and repair, genotoxic agents, Kinetoplast  
52 Associated Protein (KAPs), kDNA, symbiont-bearing trypanosomatids.

53

54

55

56

57

58

59

60

61

## 62 **Introduction**

63           The kinetoplast contains the mitochondrial DNA (kDNA) of trypanosomatids,  
64 which is arranged in a network of several thousand minicircles categorized into different  
65 classes and several dozen maxicircles that are virtually identical. Minicircles (0.5 - 10 kb)  
66 are physically connected to each other and also to maxicircles (20 - 40 kb) that are usually  
67 interwoven into the network periphery<sup>1,2</sup>. Maxicircle sequences encode components of  
68 the respiratory chain and ribosomal proteins, but first, posttranscriptional editing of the  
69 generated mRNA is required. This process is mediated in part by small noncoding guide  
70 RNAs (gRNAs) that are transcribed from minicircles<sup>3,4</sup>. The kDNA network is linked to  
71 the basal body through proteins that compose the tripartite attachment complex (TAC)<sup>5</sup>.  
72 Usually, loss of kDNA is associated with mitochondrial dysfunction, which makes this  
73 structure a potential chemotherapy target and diagnostic marker for trypanosomiasis<sup>6,7,8</sup>.

74           In contrast to most eukaryotes, mitochondrial DNA replication in trypanosomatids  
75 is regulated during the cell cycle, initiating immediately before nuclear DNA replication  
76 in S phase followed by network scission and kinetoplast division during the G2 phase.  
77 The duplication cycle of the kinetoplast occurs in four steps: kDNA synthesis; scission,  
78 when kDNA is cleaved into two networks; separation; and partitioning of kinetoplast  
79 between the daughter cells during cytokinesis<sup>9</sup>. The kDNA network replication is a  
80 complex and unusual mechanism that involves various enzymes, such as the  
81 mitochondrial topoisomerase II (mtTopo II), which detaches covalently closed  
82 minicircles from the network. Minicircle replication initiates at the kinetoflagellar zone  
83 (KFZ), which comprises the region between the kDNA facing the basal body and the  
84 inner mitochondrial membrane. At the KFZ, the minicircles duplicate as theta structures,  
85 by UMSBP, Pol 1B, and other proteins and subsequently migrate to the antipodal sites.  
86 At this kinetoplast region, a primase enables the synthesis initiation of new DNA  
87 fragments following kDNA replication that involves more than 100 enzymes, such as  
88 universal minicircle sequence-binding protein (UMSBP) and polymerases. Next, each  
89 newly replicated minicircle is reattached to the network by the mtTopoII, maintaining at  
90 least one nick/gap that is filled by proteins, such as Pol  $\beta$ -PAK and DNA ligase  $\alpha$ , prior to  
91 the network scission. Later, the duplicated network is separated by the basal body  
92 distance, since the kDNA is connected to it via the TAC structure. This minicircle  
93 replication model was primarily based on findings obtained with *Trypanosoma brucei*  
94 and *Crithidia fasciculata*<sup>4</sup>.

95           The kDNA arrangement varies according to species and developmental stages,  
96 ranging from densely packed fibers to a looser distribution in the kinetoplast matrix<sup>10,11,12</sup>.  
97 The proteins involved in this intriguing phenomenon have not been fully characterized.  
98 Kinetoplast-associated proteins (KAPs) are homologous to small basic histone H1-like  
99 proteins and nonhistone high-mobility group (HMG) box-containing proteins. KAPs have  
100 low molecular weights, are highly basic, are rich in alanine and lysine residues and  
101 contain a cleavable nine amino acid presequence involved in protein import to the  
102 kinetoplast in their amino-terminal region<sup>13</sup>. KAPs are involved in kDNA duplication,  
103 transcription, packing and topological remodeling<sup>14,15,16</sup>. KAPs can also bind to other  
104 proteins, such as UMSBP; in this case, they promote kDNA unpacking and facilitate the  
105 access of mtTopoII, which liberates minicircles from the network for replication<sup>17</sup>.

106           The first model used to study the roles played by KAPs was the monoxenic  
107 *Crithidia fasciculata*, where the disruption of the *KAP1* gene generated viable cells with  
108 a phenotype of highly condensed kDNA fibers, which was similar to that observed when  
109 trypanosomatids were treated with nalidixic acid, an inhibitor of prokaryote  
110 topoisomerase II<sup>15,18</sup>. When both *C. fasciculata* alleles for *KAP2* and *KAP3* were  
111 disrupted separately, no detectable phenotypes were generated, and the same lack of  
112 phenotypes was observed to heterozygous cells (*kap2/3*<sup>+/-</sup>), indicating a redundant  
113 function for these two encoded proteins. However, the double-knockout cells had notably  
114 slow proliferation, atypical cell morphology, an increased copy number of mRNAs  
115 encoding for ATPase and a significantly reduced respiration<sup>15</sup>. These first findings  
116 obtained with knockout cells indicated that KAPs were involved in distinct functions,  
117 such as kDNA arrangement and metabolism. Deletion of the *KAP3* gene was also  
118 performed in *Trypanosoma cruzi* by homologous recombination. Such null mutants did  
119 not exhibit changes in cell proliferation, differentiation, kDNA arrangement and  
120 infectivity, suggesting that this KAP is not essential for this parasite<sup>19</sup>. Later, the RNAi  
121 system was used to knockdown proteins associated with kDNA in *Trypanosoma brucei*.  
122 Downregulation of KAP6 promoted cell growth arrest and inhibition of covalently closed  
123 minicircle release, resulting in loss, shrinkage and disorganization of kDNA<sup>20</sup>.

124           Symbiont-harboring trypanosomatids (SHTs), such as *Angomonas deanei*  
125 (previously classified as *Crithidia deanei*<sup>21</sup>), coevolve in a mutualist relationship with a  
126 single bacterium that divides in synchronicity with other host cell structures and is usually  
127 observed close to the nucleus. During the protozoan cell cycle, the bacterium is the first

128 DNA-containing structure to divide, followed by the kinetoplast and the nucleus<sup>22,23,24</sup>.  
129 The symbiont is a gram-negative of the Alcaligenaceae family that contains a reduced  
130 genome, is enclosed by two membranes and has a very reduced peptidoglycan layer<sup>25,26,27</sup>.  
131 Such species has been used to study the kinetoplast which, in these cells, presents atypical  
132 shapes and a looser kDNA arrangement, which is more susceptible to topoisomerase  
133 inhibitors and DNA-binding drugs<sup>11,18,28,29</sup>. Recently, phylogenetic analysis showed that  
134 SHTs present an expanded repertoire of nuclear encoded KAPs and that genes for KAP4  
135 and KAP7 are present in all trypanosomatid species analyzed to date<sup>11</sup>.

136 While mitochondrial DNA is subjected to the same damage sources as nuclear  
137 DNA, the reactive oxygen species (ROS) generated by the oxidative phosphorylation  
138 metabolism usually results in higher mutation rates in the mtDNA than does damage  
139 caused to nuclear DNA. In mammalian cells, base excision repair has been described as  
140 a restoration mechanism in the mitochondrion with the identification of several  
141 glycosylases, such as MYH, NEIL1, NEIL2 and UNG1, that are involved in the response  
142 of mtDNA to oxidative damage<sup>30,31,32,33</sup>. Other proteins, such as APE1, APE2, FEN1, and  
143 DNA2, were also detected, suggesting that all steps of this repair mechanism are present  
144 in the mitochondria of mammals<sup>34,35,36,37,38</sup>. Mismatch removal activity was also  
145 identified in this organelle<sup>39</sup>, although it has not been determined which proteins are  
146 involved in this process and whether the same pathway is active in the nucleus. However,  
147 the most striking and unexpected feature in mammalian cells is the lack of DNA repair  
148 mechanisms to address UV- and cisplatin-induced lesions on the mtDNA<sup>40-42</sup>.

149 In trypanosomatids, some proteins involved in DNA repair have been described  
150 in both nuclear DNA and in kDNA metabolism. It was demonstrated that *T. cruzi* is able  
151 to remove oxidative lesions from both genomes, although damage to the kDNA remains  
152 higher than that in the nucleus<sup>43,44,45</sup>. This parasite contains DNA glycosylases that  
153 participate in the kDNA damage response<sup>43-44</sup>, as well as polymerases involved in the  
154 response to oxidative stress, such as Pol $\beta$ , Pol $\beta$ -PAK<sup>46,47</sup> and Pol $\kappa$ , which are able to  
155 interact with intermediates of the homologous recombination<sup>48</sup>. Studies in *T. brucei*  
156 showed that the bloodstream form is able to deal with damage caused by cisplatin,  
157 hydrogen peroxide and methylmethanesulfonate (MMS), suggesting that DNA repair  
158 pathways are present in the parasite mitochondrion and that TbRad51 might be crucial to  
159 the response to alkylation lesions<sup>49</sup>.

160 In the present work, for the first time, we used the CRISPR-Cas9 system to  
161 analyze the role played by KAP in a trypanosomatid protozoan. The results demonstrated  
162 that *A. deanei*  $\Delta kap4$  mutants have reduced proliferation and exhibit morphological and  
163 ultrastructural alterations. In KAP4 mutants, the kDNA network becomes highly packed  
164 and cells have atypical phenotypes including filamentous bacterium and atypical numbers  
165 arrangement of nuclei and kinetoplasts. Considering alterations in kDNA arrangement,  
166 gene deletion mutants were not more sensitive to cisplatin and UV treatment than wild-  
167 type protozoa, but these genotoxic agents interfered with cytokinesis in both cell types.  
168 Notably, cisplatin and UV lesions can be repaired in mitochondrial DNA, which suggests  
169 that there are unique DNA repair mechanisms in the trypanosomatid kinetoplast.

170

## 171 **Material and Methods**

### 172 **Cell culture**

173 The *Angomonas deanei* wild type (WT – ATCC 30255) strain was cultured in Warren's  
174 medium<sup>50</sup> supplemented with 10% fetal bovine serum. Protists were maintained by  
175 weekly passages by inoculating 10% of an established cell culture in fresh medium. WT  
176 and T7RNAPol-SpCas9 cell lines were grown at 28 °C for 24 h and cells with single or  
177 double deletions to *kap4* genes were grown for 48 h, both cases corresponded to the  
178 protozoan exponential growth phase. After this growth period, cells were used in assays  
179 or stored at 4 °C.

180

### 181 **Analysis of cell growth and viability**

182 For the growth curve, the initial cell concentration was  $1 \times 10^6$  cells/mL, and counts were  
183 made every 24 h up to 72 h. Cell density was determined by counting live protozoa in a  
184 flow cytometer, where cell size was evaluated by detection of forward scatter on an SSA  
185 detector in a BD Accuri C6 flow cytometer (Becton Dickinson Bioscience BDB, San  
186 Jose, CA, USA). The relative growth rate ( $\mu$ , expressed as h<sup>-1</sup>) of the exponential phase  
187 was estimated by an exponential function  $y = Ae^{Bx}$ , considering the parameters of  
188 culture cell density (cells/mL) vs culture time (h) of each strain, when  $B = \mu$ . Such graphics  
189 only considered the cell density from 0 h to 48 h of growth, which corresponds to the

190 exponential phase, when all assays in this study were performed. Cell duplication time  
191 (DT) was calculated according to the formula  $DT = \frac{\ln 2}{\mu}$ .  
192 To test cell viability,  $5 \times 10^6$  cells were washed once with filtered-sterilized PBS  
193 (phosphate-buffered saline) pH 7.2 and incubated for 10 min with 20  $\mu\text{g}/\text{mL}$  propidium  
194 iodide (PI). After this step, 10,000 events per sample were collected, and the fluorescence  
195 was detected on an FL-2 filter (488/630). The percentages of viable and nonviable cells  
196 were determined using control assays of life and death, respectively. To check cell death,  
197 cells were fixed in 4% paraformaldehyde for 10 min, washed with PBS, pH 7.2 and  
198 subsequently incubated with propidium iodide (PI 1:100). To control for living cells,  
199 protozoa were washed in PBS, pH 7.2, but were not incubated with PI. Cell fluorescence  
200 was detected as previously described. In such viability assays, as well as in growth curves,  
201 cells were collected on a BD Accuri C6 flow cytometer (Becton Dickinson Bioscience  
202 BDB, San Jose, CA, USA) using the manufacturer software.

203

#### 204 **Genotoxic treatment**

205 WT and AdKAP4 mutants were compared by plating  $1 \times 10^7$  cells. $\text{mL}^{-1}$  in the presence or  
206 absence of genotoxic agents. For cisplatin treatment, cells were incubated with 150 and  
207 300  $\mu\text{M}$  of the inhibitor for 1 h, washed three times with PBS at pH7.2 and resuspended  
208 in fresh medium. UVC irradiation (254 nm) was performed with a germicidal lamp at a  
209 fluence rate of 1,500  $\mu\text{J}/\text{cm}^2$  (GS GeneLinker UV Chamber, Bio-Rad). For growth curves,  
210 in all conditions, the number of surviving cells was determined at 0 h (immediately before  
211 the treatment) and after 12 and 24 h of treatment, which corresponds to the *A. deanei*  
212 exponential phase<sup>19</sup>. Experiments were performed in triplicate. The cell number was  
213 determined in a hemocytometer chamber using the erythrosine vital stain (0.4% diluted  
214 in 1x PBS) to differentiate living and dead cells. Only dead cells were stained, presenting  
215 a red color. The survival rate was calculated by comparing treated and control cells, which  
216 were employed as references (considered as 100%).

217

#### 218 **Cell cycle analysis by flow cytometry**

219 Protozoa were treated with cisplatin 150 and 300  $\mu\text{M}$  for 1 h. Next, the cells were washed  
220 twice with PBS, pH 7.2, and the culture medium was replaced as described above.



221 Protozoa were analyzed before treatment, as well as 1 h and 24 h after the incubation with  
222 the inhibitor. Approximately  $5 \times 10^6$  cells were pelleted, washed once with PBS and fixed  
223 in 0.25% paraformaldehyde at room temperature for 5 min. Next, the cells were  
224 permeabilized in 70% ethanol, in an ice bath, for 30 min and incubated with 100  $\mu\text{g}/\text{mL}$   
225 RNase and 25  $\mu\text{g}/\text{mL}$  propidium iodide at 37 °C for 30 min. After this step, 10,000 events  
226 per sample were collected, and the fluorescence was detected on an FL-2 filter (488/630)  
227 on a BD Accuri C6 flow cytometer (Becton Dickinson Bioscience BDB, San Jose, CA,  
228 USA) using the manufacturer's software. DNA histograms were analyzed with the same  
229 software.

230

## 231 **CRISPR-Cas9 gene editing**

### 232 **a - Protozoa transformation**

233 *Angomonas deanei* transfections were performed by electroporation using the Amaxa 2B  
234 system program U-033 (Human T Cell Nucleofector™ Kit - Lonza), as previously  
235 described<sup>24</sup>. Cultures were immediately split into 2 populations, and recovered for 4 hours  
236 at 26 °C before the addition of suitable antibiotics. Motile cells in both populations were  
237 counted and diluted for distribution in 96-well plates (200  $\mu\text{L}$  of 1 or 0.5 cells/well).  
238 Clones were recovered after 5-8 days. *Angomonas deanei* T7RNAPol-SpCas9 was  
239 engineered using the pTB007 plasmid previously employed for *Leishmania* species, and  
240 SpCas9 expression was confirmed by Western blotting as in Beneke et al., 2017<sup>51</sup>.  
241 Transgenic lines were maintained in the following antibiotics and respective  
242 concentrations: G418 (250  $\mu\text{g. mL}^{-1}$ ) and hygromycin (300  $\mu\text{g. mL}^{-1}$ ).

243

### 244 **b - CRISPR-Cas9 DNA fragment preparation**

245 CRISPR-facilitated mutants were obtained by transfection of PCR fragments. The  
246 sgRNA sequence was obtained from EuPaGDT<sup>52</sup>, selected based on correct on-target  
247 sequence (ADEAN\_000063100)<sup>53</sup> and fewer *A. deanei* genome off-target hits, as well as  
248 sgRNA predicted activity. The sgRNA forward oligonucleotide is designed by flanking  
249 it with the T7RNAPol promoter (upstream) and the first 20 nucleotides of the SpCas9  
250 scaffold (downstream). This oligo is combined with a universal primer containing the  
251 remaining sequence of SpCas9 backbone (OL00 - Table 1). Amplification was performed

252 in 20  $\mu$ L using 0.2 mM dNTPs, 2  $\mu$ M of each primer in Q5 reaction buffer and high-  
253 fidelity polymerase (NEB). The PCR program was set as 30 s at 98  $^{\circ}$ C followed by 35  
254 cycles of 10 s at 98  $^{\circ}$ C, 30 s at 60  $^{\circ}$ C, and 15 s at 72  $^{\circ}$ C. The repair template fragments  
255 were produced using primers containing annealing sequences compatible with pPLOT  
256 and pT plasmids<sup>51</sup> and 30 nucleotide homology arms at the 5' end of the oligonucleotide,  
257 both forward and reverse, for recombination upstream and downstream of the DNA  
258 double strand break (DSB), respectively, at the UTR of the gene. Fragments were  
259 amplified from 20 ng of pTNeo\_v1<sup>51</sup> using the same reaction buffer described above for  
260 sgRNA fragments in a final volume of 40  $\mu$ L. PCR program was 10 min at 98  $^{\circ}$ C followed  
261 by 40 cycles of 30 s at 98  $^{\circ}$ C, 30 s at 60  $^{\circ}$ C, 2 min 15 s at 72  $^{\circ}$ C, and a final elongation  
262 step of 10 min at 72  $^{\circ}$ C. Products were run on 2% (sgRNAs) or 1% (repair templates)  
263 agarose gels in 0.5% Tris-Borate-EDTA (TBE) to confirm fragment amplification and  
264 expected sizes. Primer sequences are detailed in Table 1. DNA for transfection was  
265 prepared by combining sgRNA and repair templates followed by precipitation in a one-  
266 tenth volume of 3 M NaOAc, pH 5.5 and 2.5 volumes of ice-cold absolute ethanol and  
267 washing in 70% ethanol thereafter. DNA was resuspended in 10  $\mu$ L of molecular biology  
268 grade water and immediately transfected.

269

## 270 **Diagnostic PCRs**

271 Genomic DNA (gDNA) was purified after clone cell culture amplification and kept under  
272 antibiotic selection, using the DNeasy Blood & Tissue Kit (Quiagen) following the  
273 manufacturer's instructions. PCRs were set using 50 ng of gDNA using PCR BIO HS Taq  
274 Mix Red (PCR Biosystems) and 0.4  $\mu$ M of primers to amplify the CDS locus or the  
275 integrated repair template containing the resistance marker gene (Neo). The  
276 oligonucleotides OL05+OL6 were used to detect *KAP4* presence or absence, respectively.  
277 Oligonucleotides OL05+OL07 were used to confirm integration of the repair template  
278 containing the neomycin (Neo) resistance marker at *KAP4* loci. The PCR program used  
279 was 5 min at 95  $^{\circ}$ C followed by 25 cycles of 30 s at 95  $^{\circ}$ C, 30 s at 55  $^{\circ}$ C, 20 s at 72  $^{\circ}$ C  
280 and a final elongation step of 5 min at 72  $^{\circ}$ C. Reactions were directly run in a 0.8%  
281 agarose gel in TBE to confirm genetic manipulation by comparing the presence or  
282 absence of WT and mutants PCR products. Primer sequences are detailed in Table 1.

283

## 284 **Fluorescence microscopy**

### 285 **a - DAPI Staining**

286 Protozoa were collected by centrifugation at 2000 ×g, washed once with PBS (phosphate  
287 buffered saline) pH 7.4, fixed in 4% paraformaldehyde in the same solution, and mounted  
288 on poly-L-lysine-coated circular microscope coverslips (14 mm diameter), next, the  
289 slides were washed with PBS and incubated with 10 µg/ml 4',6-diamidino- 2-  
290 phenylindole (DAPI, from Molecular Probes, Oregon, USA) for 10 min. After washing  
291 with PBS, slides were mounted using ProLong Gold (Molecular Probes), and visualized  
292 using a TCS SP5 confocal laser scanning microscope (Leica, Germany). Confocal images  
293 were obtained using an HCX PL APO 60× objective for light microscope oil immersion  
294 with a numerical aperture of 1.4. Optical sections obtained from the whole cell were  
295 transformed into 2D images by maximum projection in the manufacturer's software  
296 (LAS-X). The cellular patterns were determined by counting DNA-containing structures  
297 as nuclei, kinetoplasts and symbionts. Symbiont division was evaluated based on its form  
298 as described previously<sup>22,24</sup>. Analyses were based on counts of 1,000 cells of WT and  
299 KAP4 mutants.

300

### 301 **b - Immunofluorescence with anti-porin antibody**

302 Protozoa were washed in PBS and fixed with freshly prepared 2% formaldehyde diluted  
303 in PBS, for 1 h. After fixation, cells were adhered to poly-L-lysine-coated microscope  
304 coverslips and permeabilized with 4% Nonidet P-40 (NP-40) diluted in PBS for 45 min.  
305 Slides were incubated in blocking solution containing 1.5% bovine serum albumin  
306 (BSA), 0.5% teleostean gelatin (Sigma Aldrich), and 0.02% Tween 20 diluted in PBS.  
307 Next, slides were incubated for 1 h with antibody produced against the symbiont porin<sup>54</sup>  
308 diluted 1:10 in blocking solution. After that step, the cells were washed with PBS and  
309 incubated for 45 min with Alexa488-conjugated anti-mouse IgG (Molecular Probes,  
310 USA) diluted 1:200 in blocking solution. Slides were mounted using the anti-fading  
311 reagent ProLong Gold containing 5 µg. mL<sup>-1</sup> of DAPI (4',6-diamidino-2-phenylindole,  
312 MolecularProbes). Serial image stacks (0.36-µm Z-increment) were collected at 64x (oil  
313 immersion 1.4 NA) on an Elyra PS.1 microscope (Carl Zeiss) and three-  
314 dimensional projections were obtained on the Zen Black program (Carl Zeiss).

315

### 316 **c - *In situ* labeling of kDNA networks**

317 Cells were centrifuged, washed, and fixed in 2% paraformaldehyde diluted in PBS for 5  
318 min. Next, cells were adhered to poly-L-lysine-coated slides for 10 min and washed twice  
319 in PBS containing 0.1 M glycine for 5 min. After permeabilization in methanol for 1 h  
320 at 20 °C, cells were rehydrated with three washes in PBS for 5 min and incubated for 60  
321 min at room temperature in 25 µl of reaction solution containing: TdT reaction buffer  
322 (Roche Applied Science), 2.0 mM CoCl<sub>2</sub>, 10 µM dATP, 2.5 µM Alexa Fluor 488-dUTP  
323 (Molecular Probes) and 10 units of TdT (Roche Applied Science). The reaction was  
324 stopped with three washes in 2xSSC for 5 min. Slides were mounted using the anti-fading  
325 reagent ProLong Gold containing 5 µg. mL<sup>-1</sup> DAPI (4',6-diamidino-2-phenylindole,  
326 MolecularProbes). Slides were examined on an Axiobserver microscope (Carl Zeiss), and  
327 images were collected at 100x (oil immersion 1.4 NA). Analyses were based on counts  
328 of 1,000 cells of WT and KAP4 mutants considering the kDNA replication as described  
329 by Liu and Englund (2007)<sup>55</sup>.

330

### 331 **Electron Microscopy**

#### 332 **a - Scanning electron microscopy (SEM)**

333 Sample processing was performed using glass coverslips precoated with 1 mg/mL poly-  
334 L-lysine. Protozoa were fixed for 1 h in 2.5% glutaraldehyde diluted in 0.1 M cacodylate  
335 buffer pH 7.2. Cells were subsequently adhered to coverslips, postfixed for 1 h with 1%  
336 osmium tetroxide diluted in cacodylate buffer, and dehydrated in a graded alcohol series  
337 (50%, 70%, 90%, and two exchanges of 100% ethanol for 10 min each step). Samples  
338 were critical-point dried in a Leica EM CPD030 apparatus (Leica, Wetzlar, Germany).  
339 Specimens were sputtered with gold in a Balzers FL9496 unit (Postfach 1000 FL-9496  
340 Balzers Liechtenstein) and observed in an EVO 40 VP SEM (Zeiss, Germany). In all  
341 assays performed, approximately 500 cells were observed.

342

#### 343 **b - Transmission electron microscopy (TEM)**

344 Protozoa were fixed for 1 h in 2.5% type II glutaraldehyde (Sigma, Missouri, USA)  
345 diluted in 0.1 M cacodylate buffer, pH 7.2. The protozoa were washed twice in cacodylate  
346 buffer and postfixed (1% osmium tetroxide, 0.8% potassium ferrocyanide, 5 mM calcium  
347 chloride diluted in 0.1 M cacodylate buffer) for 1 h. Samples were then washed in

348 cacodylate buffer, dehydrated in a graded series of acetone solutions (50%, 70%, 90%,  
349 and two exchanges of 100% acetone) for 10 min at each step, and embedded in Polybed  
350 resin. Ultrathin sections were stained with 5% uranyl acetate for 45 min and lead citrate  
351 for 5 min before observation in a Jeol 1200 EX TEM operating at 80 kV. In all assays  
352 performed, approximately 500 cells were analyzed.

353

### 354 **Damage quantification by long-range qPCR analysis**

355 Parasite cultures were treated with the respective drug as reported above. After treatment,  
356  $1 \times 10^8$  cells were harvested by centrifugation at 3,000  $xg$  for 5 min at the time points after  
357 treatment indicated on the graph. The first time point (0 h) was collected immediately  
358 after the end of UV radiation exposure, and after the washes to remove cisplatin from the  
359 media in cisplatin treatment. DNA extraction was performed by using the QIamp® DNA  
360 Mini and Blood Mini Kit (Qiagen, cat: 51104) protocol for tissue extraction.

361 Amplification was performed using a Kappa LongRange HotStart PCR Kit (Sigma, cat:  
362 KK3501). Specific primers for the mitochondrial coding region were used and are listed  
363 in Table 1. Amplification of the large mitochondrial fragment (approximately 10 kB) was  
364 performed by using primers qPCRMitF and qPCRMitR. Amplification of the small  
365 mitochondrial fragment (250 bp) was performed by using the primers qPCRMitSmF and  
366 qPCRMitR. For the nuclear fragment analyses, the amplification of the larger fragment  
367 was performed using the primers qPCRNucF and qPCRNucR. The smaller fragment was  
368 amplified using the primers qPCRNucSmF and qPCRNucR.

369 The assay consists of the comparison of the amount of amplified material of treated cells  
370 with the amount of amplified material within nontreated cells. The smaller fragment was  
371 used to normalize the amplification of the large fragments and to avoid any bias from  
372 uneven loading of template DNA among the various PCRs. The normalized value of  
373 treated and nontreated cells was compared, and the relative amplification was  
374 subsequently calculated. These values were used to estimate the average number of  
375 lesions/10 kb of the mitochondrial genome using a Poisson distribution. All the results  
376 presented are the mean of two technical replicates of amplification and two different  
377 biological experiments. Details of the data analysis can be found in the literature<sup>56</sup>.

### 378 **Results**

379 To allow genetic manipulation in *A. deanei* facilitated by CRISPR-Cas9, we first  
380 generated an *A. deanei* mutant expressing SpCas9 and T7RNAPol by transfecting log-  
381 phase cells with the pTB007, generously provided by Dr. Eva Gluenz and previously used  
382 to generate a similar mutant in *Leishmania* sp.<sup>52</sup>. Western blotting confirmed SpCas9  
383 expression in the mutants generated, using *L. mexicana* T7RNAPol-SpCas9 as a control  
384 (Supplementary Material 1).

385 To verify whether the expression of SpCas9 in the AdT7RNAPol-SpCas9 strain  
386 could constitutively cut nonspecific sites, long-range qPCR quantification was performed  
387 to determine the amount of possible accumulation of DNA damage in those cells. WT  
388 protozoa were used as a controls, since they do not contain the cassette construction for  
389 the SpCas9 expression. If SpCas9 generated nonspecific DNA damage, it was expected  
390 to produce a difference between the amplification ratio of the genetically modified strain  
391 in comparison with WT cells. The amplification for both strains was approxemetly 1,  
392 indicating that the expression of SpCas9 on *A. deanei* did not generate DNA strand breaks  
393 in a nonspecific manner in either nuclear or mitochondrial genomes (Figure 1, a and b).  
394 The confirmed mutant had a regular morphology, and SpCas9 expression was well  
395 tolerated. To delete *KAP4*, *A. deanei* was cotransfected with a repair template containing  
396 the neomycin resistance gene and 30 nt homologous to flanking *KAP4* UTRs', and 2  
397 sgRNA templates were expressed *in vivo* by T7 RNA polymerase to insert DSBs at the  
398 5' and 3' ends of the gene. Cells were kept under G418 pressure and mutants were  
399 confirmed by diagnostic PCR to detect the resistance cassette integration and *KAP4*  
400 deletion (Figure 1c). We were able to disrupt one or both alleles of *KAP4* by integrating  
401 a resistance marker (*NEO*), and enabling selection with neomycin (Figure 1d), thereby  
402 successfully validating our system.

403 Analyses of cell proliferation showed that WT, T7RNAPol-SpCas9 and *KAP4*  
404 mutants cultivated for 48 h, which corresponds to the peak of exponential phase,  
405 presented different proliferation profiles: when compared to WT protozoa, T7RNAPol-  
406 SpCas9 strain had a reduction of 19% in proliferation, whereas these values were  
407 equivalent to 67% and 69% to gene-deficient cells for one or both alleles of *KAP4*,  
408 respectively (Figure 1e). The duplication times of WT and T7RNAPol-SpCas9 were  
409 similar and equivalent to 7.1 and 7.4 h, respectively, whereas values obtained for  $\Delta kap4$   
410 with single or double deletions were 9.3 hours and 9.5 hours, respectively (Figure 1f).  
411 Although WT cells, as well as the T7RNAPol-SpCas9 background and *KAP4* mutants,

412 exhibited distinct decreases in proliferation after 48 h (Figure 1e), the viability rate after  
413 72 h of cultivation was similar to that of all cell types, that is, approximately around 98.5%  
414 (Figure 1g).

415 The morphological and ultrastructural analyses in this study used cells cultivated  
416 for 24 h, which is equivalent to the exponential growth phase of *A. deanei*, whose  
417 generation time is equivalent to 6 h. Transmission electron microscopy images showed  
418 that as in other trypanosomatids, the nucleus usually occupies a central position in the cell  
419 body and contains a nucleolus surrounded by heterochromatin, which is also observed at  
420 the nuclear periphery. The symbiont was usually observed close to the host cell nucleus  
421 and delimited by two membranes (Figure 2a). *A. deanei* WT displays a trapezoidal  
422 kinetoplast containing a looser arrangement of the kDNA fibers in the central area and a  
423 more densely packed array in the region that faces the TAC and connects the  
424 mitochondrial DNA to the basal body (Figure 2b). This same phenotype was observed in  
425 the CRISPR-Cas9 background cell line that did not have alterations in kinetoplast shape  
426 or kDNA arrangement (Figure 2, d-e). Scanning electron microscopy demonstrated that  
427 the WT and CRISPR-Cas9 background strains presented the typical choanomastigotes of  
428 the *Angomonas* genus. The smooth cell surface often exhibited gentle undulations that  
429 corresponded to mitochondrial branches (Figure 2, c-f).

430 In cells with a single deletion (*kap4<sup>+/-</sup>*) the kinetoplast shape was maintained;  
431 however, kDNA fibers of the central area were broken in most cells, and the kinetoplast  
432 network was determined to be more condensed as a whole than those observed in control  
433 cells. In some instances, the nucleus presented matrix loss and a more condensed  
434 chromatin (Figure 2, g and i). Such protozoa showed unusually elongated symbionts,  
435 indicating that bacterial division was impaired (Figure 2h). In *KAP4* null mutants, cells  
436 with division impairment phenotype usually presented two flagella in the same flagellar  
437 pocket (Figure 2m). The symbiotic bacterium was also affected in these cells, which  
438 presented filamentous forms surrounded by small vacuoles (Figure 2n). The kDNA  
439 packing was severely compromised in the whole network, especially in the central area  
440 (Figure 2o). Alterations in the nuclear ultrastructure were rarely observed.

441 As a next step, analysis by scanning electron microscopy was performed by  
442 comparing *KAP4* mutants and WT protozoa. Cells with a single gene deletion (*kap4<sup>+/-</sup>*)  
443 had alterations in morphology, with many protozoa showing a round shape with a  
444 shortened flagellum (Figure 2j, white arrow). Part of the culture presented body shape

445 asymmetry during division (Figure 2j, gray arrow), which resulted in the generation of  
446 daughter cells with different dimensions (Figure 2k). Protozoa with multiple cell bodies  
447 and flagella were also observed, indicating cytokinesis impairment (Figure 2l). Null  
448 mutants also presented morphological alterations, such as cell body shortening and  
449 flagellar length reduction (Figure 2p). A high number of cells with impaired cytokinesis  
450 was observed, thereby generating a popcorn-like phenotype (Figure 2, q-r).

451 Analyses of cellular patterns were performed in *A. deanei* labeled with DAPI and  
452 with an anti-porin antibody that recognizes the endosymbiont, considering the number of  
453 nuclei, kinetoplasts and symbionts, as well as the shape of the bacterium (Figure 3). As  
454 expected, in asynchronous cultures of WT cells, approximately 30%, presented one rod-  
455 shaped symbiont, one kinetoplast and one nucleus (1S1K1N). Most cells, that is,  
456 approximately 50%, also presented 1S1K1N; however, the symbiont presented a  
457 constricted or dividing format. The other part of the culture, approximately 20%, was  
458 composed of cells containing two rod-shaped symbionts. Such protozoa presented one or  
459 two kinetoplasts and nuclei; however, kinetoplast division was always observed before  
460 the karyokinesis. In *KAP4* mutants cultivated for 24 h, protozoa presented atypical  
461 phenotypes as two nuclei, one kinetoplast and one filamentous symbiont (1Sf2N1K) or  
462 two nuclei, two kinetoplasts and one filamentous symbiont (1Sf2N2K), an indication of  
463 kDNA division and cytokinesis blockage, respectively (Figure 3, a-d). In *KAP4* mutants  
464 cultivated for 24 h, filamentous symbionts were observed in 3% *kap4*<sup>+/-</sup> cells and in 54%  
465 of *kap4*<sup>-/-</sup> protozoa, exhibiting bacterium division impairment (Figure 3e).

466 The counting of cell patterns in *KAP4* mutants showed that the percentage of  
467 filamentous symbionts was higher in cells containing one bacterium, one nucleus and one  
468 kinetoplast (1Sf1N1K) than in cells containing two nuclei or two kinetoplasts, indicating  
469 that as the cell cycle progresses, the symbiont filamentation increases, eventually leading  
470 to bacterial lysis. The percentage of cells containing one filamentous symbiont, two nuclei  
471 and one kinetoplast (1Sf2N1K) was almost three times higher than in *kap4*<sup>-/-</sup> protozoa  
472 when compared to *kap4*<sup>+/-</sup> cells, indicating that in the double mutant, kinetoplast division  
473 was more affected (Figure 3f). To check whether the *KAP4* mutant phenotype has an  
474 impact on kDNA replication, assays of dUTP incorporation by the deoxynucleotidyl  
475 transferase terminal (TdT) were performed. The results showed that the percentage of  
476 cells with the kDNA in the early replication stage was 62.5% lower in cells containing  
477 deletions of both *KAP4* genes than in WT protozoa. During this stage, the kinetoplast



478 exhibits strong labeling in the antipodal sites but little labeling in the kDNA network  
479 (Figure 3g).

480           Considering the structural results obtained in this work, we assumed that *A. deanei*  
481 KAP4 could participate in kDNA metabolism. To confirm this hypothesis, WT and  
482 mutant cells were exposed to cisplatin or UV radiation to verify the cell response to DNA  
483 damage. These agents cause distortions in the DNA that can impair transcription and  
484 replication, with cisplatin lesions being more effective than UV light<sup>48, 49, 50, 51, 52</sup>. Protozoa  
485 that had one or both *KAP4* genes deleted were able to grow after treatment with cisplatin  
486 or exposure to UV, although in cisplatin treatment, the mutant cells presented a slight  
487 decrease in cell proliferation compared to the WT strain after 12 hours of treatment,  
488 especially the single gene-deficient mutant treated with the highest inhibitor  
489 concentration (Figure 4, a-d).

490           Considering the cellular morphology and cellular organization, microscopy  
491 analyses were performed to test whether *KAP4* mutants presented atypical phenotypes in  
492 relation to WT cells after cisplatin treatment. This compound interacts with DNA and  
493 proteins and forms intrastrand or interstrand DNA crosslinks that cause distortions in the  
494 double helix, thereby blocking duplication and transcription. Transmission electron  
495 microscopy images showed that WT cells did not present nuclear or kinetoplast changes  
496 after incubation with cisplatin, even when a higher drug concentration (300  $\mu$ M) was used  
497 (Figure 5, a-c). The same phenomenon was observed in the background T7RNAPol-  
498 SpCas9 cell line (data not shown). Similarly, *KAP4* mutants did not display topological  
499 rearrangement on the kDNA network compared to WT cells treated with cisplatin (Figure  
500 5, h and m). However, other cellular structures suffered alterations in mutant protozoa. In  
501 *kap4*<sup>+/−</sup> cells, nuclear DNA unpacking was observed, as well as myelin figures in the  
502 cytoplasm (Figure 5f, black arrow) and mitochondrial swelling. The abundance of the  
503 endoplasmic reticulum was noted and also its frequent association with the symbiont,  
504 which sometimes was seen surrounded by this organelle, suggested an autophagic process  
505 (Figure 5f, arrowheads). The symbiont also displayed matrix loss and alterations in its  
506 DNA condensation (Figure 5g, white arrows). In null mutants treated with 300  $\mu$ M  
507 cisplatin, the primary ultrastructural alteration was observed in the symbiont that  
508 presented membrane convolutions (Figure 5k, arrow), matrix loss and densely packed  
509 DNA fibers (Figure 5l, white arrows). It is also worthwhile to mention the presence of  
510 vacuoles around the symbiont, indicating that the bacterium had lysed (Figure 5, k-l).

511 Analyses by SEM showed that cultures of *A. deanei* WT cells presented a higher  
512 incidence of rounded protozoa with a shortening flagellum after treatment with 150 and  
513 300  $\mu\text{M}$  cisplatin for 24 h (Figure 5, d-e). This phenotype was also observed in mutant  
514 cells after treatment with both concentrations (Figure 5, i-j, n-o, white arrowheads).  
515 Protozoa presenting a fat cell-like phenotype and lacking the flagellum (Figure 5i, white  
516 arrow) were observed after treatment with 150  $\mu\text{M}$  cisplatin for 24 h. After using 300  $\mu\text{M}$   
517 of this drug, protozoa with the cytokinesis phenotype were observed more frequently  
518 (Figure 5j), indicating division impairment, as well as plasma membrane blebs at the  
519 posterior end of the cell body (Figure 5o). Protozoa that had one allele deleted seemed to  
520 have their morphology more affected than null mutant when treated with this genotoxic  
521 agent.

522 Cells subjected to cisplatin treatment presented atypical phenotypes, as  
523 demonstrated by fluorescence microscopy analysis. When treated with the lower inhibitor  
524 concentration (150  $\mu\text{M}$ ), WT trypanosomatids presented rounded shapes with a reduced  
525 flagellum length and the fat cell phenotype. Symbionts were seen in the filamentous  
526 format, presenting several nucleoids (Figure 6, a-a"). Mutants for *KAP4* treated with  
527 cisplatin also presented filamentous bacterium, but in this case, protozoa lacking the  
528 bacterium were also observed, as well as cells presenting two nuclei and one kinetoplast  
529 (Figure 6, b-b" and c-c"). Next, we counted the number of protozoa containing a  
530 filamentous bacterium after cisplatin treatment for 24 h. In WT *A. deanei*, filamentous  
531 bacteria were not identified in non-treated cells, as previously demonstrated. However,  
532 after incubation with 150  $\mu\text{M}$  and 300  $\mu\text{M}$  of cisplatin, 14% and 3% of the cells showed  
533 filamentous symbionts, respectively. In *kap4<sup>+/-</sup>* protozoa, when both concentrations of  
534 cisplatin were used, the percentage of filamentous bacteria was similar, that is,  
535 approximately 2%. In the null mutant (*kap4<sup>-/-</sup>*), values were equivalent to 14% and 8%,  
536 respectively (Figure 6d).

537 These results indicate that treatment with cisplatin induced symbiont  
538 filamentation and that a higher concentration of the inhibitor (300  $\mu\text{M}$ ) augmented  
539 symbiont lysis, as also suggested by transmission electron microscopy data. Counting of  
540 cellular patterns demonstrated that after treatment with cisplatin, the highest percentage  
541 of bacterial filamentation was present in the double mutant cells containing one nucleus  
542 and one kinetoplast (1Fs1N1K). In these cells, the percentage of protozoa with a  
543 filamentous symbiont decreased in a concentration-dependent manner. The percentage of

544 protozoa with bacterial filamentation also decreased with the progression of the cell cycle,  
545 as in cells containing two nuclei, reinforcing the notion of the bacterial lysis. Taken  
546 together, these data indicate that somehow genotoxic agents alter the cell division pattern  
547 in *A. deanei* and that this effect is exacerbated in mutant cells (Figure 6e). Cisplatin can  
548 block replication and trigger checkpoints at the end of S phase and the beginning of G2  
549 to repair lesions, thereby causing cell cycle arrest. However, when cells treated with  
550 cisplatin were submitted to flow cytometry analysis, they did not show cell cycle  
551 alterations in relation to control cells, even after treatment with 300  $\mu$ M for 24 h  
552 (Supplementary Figure 2).

553         The susceptibility of WT and mutant cells to UV radiation was also verified. Thus,  
554 protozoa were subjected to UV-C irradiation, which affects the DNA replication and  
555 transcription and can be repaired by nucleotide excision. Ultrastructural and  
556 morphological analyses were performed after 24 h of protozoa irradiation at 1500  $\mu$ J/m<sup>2</sup>.  
557 The results obtained by transmission electron microscopy were similar to those observed  
558 for WT and *KAP4* mutant cells treated with cisplatin: nuclear DNA and kDNA did not  
559 suffer additional topological alterations in relation to nonirradiated cells (Figure 7, a-b, f-  
560 g, and k), and a close association of the ER with the symbiont occurred frequently,  
561 strongly indicating autophagy (Figure 7, a, f, and k, white arrowheads). Notably, after  
562 irradiation, mutant cells presented bacteria with a higher DNA condensation (Figure 7, a,  
563 g, and k, white arrows). Furthermore, polynucleated cells were observed (Figure 7l).

564         Scanning electron microscopy analyses showed that WT protozoa suffered  
565 morphological alterations after irradiation, exhibiting wrinkled cell surfaces and irregular  
566 forms that indicated cytokinesis impairment (Figure 7, c-e). In single- and double-*KAP4*-  
567 deleted mutants, the morphological modifications were exacerbated: many protozoa  
568 presented multiple interconnected cell bodies, reinforcing the notion that cytokinesis was  
569 blocked (Figure 7, h-i). Such cells also presented wrinkled surfaces, and the flagellum  
570 was absent in some instances (Figure 7, h and j, white arrows), as also observed in null  
571 mutants (Figure 7, m and o, white arrows). In this last case, a high number of round cells  
572 were also observed (Figure 7, m-o).

573         Irradiated protozoa were also labeled with DAPI, exhibiting atypical phenotypes  
574 that were compatible with asymmetric division and cytokinesis impairment, such as the  
575 presence of one kinetoplast and two nuclei in cells containing two symbionts (Figure 8a)  
576 and dyskinetoplastic cells. Such morphotypes were observed in WT cells, as well as in

577 mutant cells (Figure 8b). Protozoa with filamentous bacterium were observed more  
578 frequently in WT cells than in *KAP4* mutants, on which symbiont division was probably  
579 more strongly affected. The absence of the symbiont was observed in null mutants (Figure  
580 8c), which may have been related to the possible occurrence of autophagy, in this case, a  
581 symbiophagy, that generated aposymbiotic cells, as suggested by transmission electron  
582 microscopy. The very reduced number of WT cells presenting filamentous symbionts  
583 (1.4%) and the absence of this phenotype in mutant cells reinforced this notion (Figure  
584 8d). The percentage of irradiated protozoa presenting atypical phenotypes was low in all  
585 cell types (Figure 8e).

586 To verify whether *KAP4* was involved in kDNA repair, mutant and wild-type cells  
587 of *A. deanei* cells were treated with cisplatin and UV radiation, as described before, and  
588 DNA repair kinetics were measured by long-range qPCR assay. After treatment with 300  
589  $\mu$ M cisplatin, WT and both mutant strains presented the same levels of DNA damage on  
590 the kDNA, which was approximately 1.5 lesions/10 kB. The repair kinetics were very  
591 similar for all cell types: after 3 h of treatment, levels of kDNA damage were almost  
592 undetectable, reaching the slowest point after 6 h (Figure 9 a-b, Supplementary Material  
593 3). A similar phenotype was observed for the UV radiation. The levels and DNA repair  
594 kinetics of mutant cells were very similar to those observed in WT cells. After 1 h of  
595 treatment, most damage had already been repaired, although it required 3 h after UV  
596 radiation to reach the same level of repair that was observed in cisplatin-treated cells, with  
597 the lowest point being observed at 6 h (Figure 9, c-d). Taken together, these results  
598 demonstrate that *KAP4* was not directly involved in the removal of DNA damage  
599 generated by cisplatin and UV radiation but, notably, show that lesions generated by both  
600 genotoxic agents could be repaired in mitochondrial DNA (Figure 9, a-d).

601

## 602 **Discussion**

603 In recent decades, *A. deanei* has been used as a model for endosymbiosis and the  
604 origin of organelles. Genome sequencing is available<sup>26,27,62</sup>, and molecular tools for gene  
605 function studies were developed, although with limited use on studies of genes essentially  
606 and symbiosis maintenance<sup>24,63</sup>. The recent application of highly efficient CRISPR-Cas9  
607 protocols to other trypanosomatids, such as *Leishmania* and *T. cruzi*, accelerated  
608 functional studies with gene deletion<sup>51,63,64</sup>. In this study, for the first time, we describe

609 gene depletion in an endosymbiont-harboring trypanosomatid. Phylogenetic proximity  
610 with *Leishmania* enabled the successful application of the CRISPR-Cas9 system  
611 developed by Beneke and colleagues (2017)<sup>51</sup> to *A. deanei*, resulting in efficient deletion  
612 of *KAP4*, a kinetoplast associated protein present in all trypanosomatids so far analyzed<sup>9</sup>.

613 KAPs can neutralize the negative DNA charge, thus facilitating the interaction of  
614 mitochondrial proteins with kDNA, as those involved in replication and transcription. In  
615 this work, deletion of *A. deanei KAP4* generated trypanosomatids with reduced cell  
616 proliferation and generated cells with atypical phenotypes, as those presenting two nuclei  
617 and one kinetoplast, as well as cytokinesis impairment. Cells containing aberrant numbers  
618 of nucleus and kinetoplast were also observed in null mutants of *C. fasciculata* for *KAP2*  
619 and *KAP3* that presented cell division block<sup>16</sup>. In *T. brucei*, the RNAi knockdown of a  
620 kDNA associated protein, resulted in reduced growth and in the appearance of  
621 dyskinetoplastic cells<sup>64</sup>. These results reinforce the importance of KAPs to cell  
622 proliferation and kDNA network replication in order to guarantee that each new protozoa  
623 will receive one kinetoplast during trypanosomatid division.

624 The coordinated division of the symbiont with the host cell nucleus was previously  
625 demonstrated in *A. deanei* and in *Strigomonas culicis*, another symbiont-harboring  
626 trypanosomatid<sup>22-24</sup>. In the present work, it was interesting to observe in *KAP4* mutant  
627 cells that the kDNA condensation, which is associated with kinetoplast replication  
628 impediment, resulted in symbiont filamentation. This filamentation occurred most  
629 frequently in mutant with two nuclei and one kinetoplast. Consistent with this notion,  
630 TdT labeling showed a lower percentage of *kap4*<sup>-/-</sup> cells in the early replication phase when  
631 compared to the WT protozoa, indicating that in such cells the mitochondrial DNA  
632 replication was delayed or even impaired. Since kDNA loss resulting in dyskinetoplastic  
633 protozoa was not observed, it can be assumed that the impediment of mitochondrion DNA  
634 replication promoted cytokinesis blockage. Taken together, the results indicate that  
635 bacterial division is also coordinated with kinetoplast replication, but further studies are  
636 essential to confirm this hypothesis. Cell cycle checkpoints are not well established for  
637 most trypanosomatids species, nor are the factors that coordinate the equal partitioning of  
638 single copy organelles to daughter cells. Such questions are best studied in *T. brucei*,  
639 especially by investigating the role of protein kinases in cell cycle progression, organelle  
640 positioning and protozoan morphology<sup>66,67,68,69</sup>. Recently, it was shown that *T. brucei*  
641 UMSBP2, which is involved in kDNA replication and segregation, is also localized at

642 telomeres. The RNAi system showed that this protein not only participates in nuclear  
643 division but also plays a role in the coordinated replication of DNA-containing  
644 organelles<sup>70</sup>.

645 In *A. deanei* *KAP4* mutants, the high level of kDNA packing was associated with a  
646 delay in cell proliferation and a delay of kDNA replication at the early stage, when the  
647 covalently closed minicircles are released from the network to initiate replication into the  
648 KFZ and then migrate to antipodal sites, where this process continues<sup>4</sup>. Previously, it was  
649 shown that the downmodulation of *T. brucei* P93, a kDNA-associated protein localized  
650 in antipodal sites, resulted in loss of gapped minicircles and consequently in the network  
651 reduction<sup>71</sup>. Similarly, in TbKAP6 RNAi cells, the levels of total minicircles and  
652 maxicircles decreased the total amount of nicked/gapped minicircles. In such cells, the  
653 kinetoplast presented network shrinkage or elongation, but in both cases, two basal bodies  
654 could be identified, indicating failures in kDNA replication and scission. Conversely,  
655 protozoa overexpressing TbKAP6 minicircle decatenation were enhanced, indicating that  
656 a controlled expression of this protein is required for proper kDNA replication<sup>20</sup>.

657 The kDNA arrangement and metabolism are the result of the coordinated activity  
658 of a set of mitochondrial proteins that serve different functions. In addition to KAPs, other  
659 proteins are involved in the kDNA replication, such as the minicircle replication factor  
660 (MiRF172), which is supposedly involved in the reattachment of replicated minicircles  
661 to the kDNA disc. Once depleted, *T. brucei* cells presented reduced kDNA content or  
662 even a dyskinetoplastic phenotype<sup>72</sup>. Downregulation of mitochondrial heat shock  
663 proteins 70 and 40 also showed impairment of minicircle replication and loss of kDNA,  
664 demonstrating the importance of chaperones to the maintenance of the kinetoplast as a  
665 cellular structure<sup>73</sup>. In the present work, the generation of dyskinetoplastic cells was not  
666 observed among *KAP4* mutants. Although the gene deletion promoted increased kDNA  
667 compaction, the data obtained by qPCR did not indicate loss of mitochondrial DNA. In  
668 UV-irradiated protozoa, a very low percentage of cells without a kinetoplasts was  
669 observed.

670 The DNA repair kinetics showed no differences between *KAP4* mutant cells and  
671 the WT strain. In both cases, protozoa were able to efficiently repair the damage generated  
672 by cisplatin and UV radiation. In addition, differences in the long-term survival of these  
673 cells were not observed. For both genotoxic agent treatments, the kDNA accumulated the  
674 same amounts of lesions in WT or *KAP4* mutant cells, suggesting that the topological

675 alterations observed in the kinetoplast network did not affect the susceptibility to DNA  
676 damage. It is well established that damage generated by UV radiation and cisplatin is not  
677 repaired in humans and other mammalian cells<sup>40,41</sup>. Notably, in *A. deanei*, damage caused  
678 by both genotoxic agents on the kDNA was repaired, representing the first demonstration  
679 of this type of repair in mitochondrial DNA. The repair kinetics observed in this instance  
680 are not related to the kDNA loss, since the number of dyskinetoplastic cells after  
681 genotoxic treatment is negligible.

682 Notably, the DNA repair kinetics were very similar when cisplatin was tested in  
683 WT and mutant cells, and the same phenomenon was observed for UV radiation.  
684 However, accentuated differences were observed when comparing the two treatments:  
685 DNA repair by cisplatin was very fast; thus, after 1 h, most lesions were already repaired,  
686 whereas for UV radiation damage, the kinetic is slower. Although it is described that  
687 lesions caused by UV and cisplatin are mainly repaired by the nucleotide excision repair  
688 pathway, the kinetics observed in this work strongly suggest that lesions caused by each  
689 genotoxic treatment activated different and specific responses in *A. deanei*. It is well-  
690 known that lesions that block transcription are repaired very quickly compared to other  
691 types of lesions. It has also been also reported that the main lesion caused by UV light  
692 (thymine dimers) can be tolerated by RNA polymerase<sup>74,75</sup>. In trypanosomatids that  
693 present a single mitochondrion, it is possible that a DNA repair pathway associated with  
694 transcription exists. The repair of UV lesions may also be associated with the  
695 recombination process. In *T. brucei*, it was seen that cells deficient in the Rad51 gene are  
696 not able to adequately repair lesions caused by methyl methanesulfonate (MMS)<sup>49,76,77</sup>.

697 Our structural analyses using microscopy techniques showed distinct atypical  
698 phenotypes after treatment with cisplatin or ultraviolet radiation. This phenomenon may  
699 be observed because cisplatin can cause more toxic injuries that culminate in cell death.  
700 Accordingly, mutant protozoa have higher sensitivity to elevated concentrations of  
701 cisplatin and lower percentages of cells containing duplicated nuclei and kinetoplasts than  
702 WT or UV-irradiated cells. In mutant cells, this inhibitor promoted a decrease in  
703 proliferation and in the number of filamentous symbionts, indicating bacterium lysis.  
704 Notably, the cell morphology and growth of KAP4 single allele deletion mutants were  
705 more affected by high doses of cisplatin than those of the null mutant cells. Since KAP4  
706 is not an essential protein, it cannot be ruled out that an adaptation process has occurred  
707 in cells where both copies of the genes were deleted. A similar phenomenon was observed

708 in null mutants of *Trypanosoma cruzi* and *Trypanosoma brucei* for the MSH2 gene, which  
709 encodes a central component of the eukaryotic DNA mismatch repair (MMR) pathway<sup>78</sup>.

710 In this work, we demonstrated for the first time that the CRISPR-Cas9 system can  
711 be used with success to delete genes in *A. deanei*. KAP4 is not an essential protein, but it  
712 is involved in the kDNA compaction, leading to the appearance of cells with atypical  
713 phenotypes, such as symbiont filamentation and the appearance of two nuclei and one  
714 kinetoplast. This protein does not seem to participate in the mitochondrial DNA repair  
715 process; however, lesions caused by cisplatin and UV radiation are repaired in the kDNA  
716 of this protozoan. The repair kinetics are different for each genotoxic agent, indicating  
717 that different pathways are used to repair the lesions. In the case of cisplatin, repair may  
718 be associated with transcription.

## 719 References

- 720 1. Lukes J, *et al.* Kinetoplast DNA Network: Evolution of an Improbable Structure  
721 *Eukaryot Cell*. **1**(4): 495–502. <https://doi.org/10.1128/ec.1.4.495-502.2002> (2002)
- 722 2. Hajduk SL, Klein VA, Englund PT. Replication of kinetoplast DNA maxicircles. *Cell*  
723 **36**(2), 483–492. [https://doi.org/10.1016/0092-8674\(84\)90241-1](https://doi.org/10.1016/0092-8674(84)90241-1) (1984)
- 724 3. Hajduk S & Ochsenreiter T. RNA editing in kinetoplastids. *RNA Biol*. **7**(2):229-236.  
725 <https://doi:10.4161/rna.7.2.11393> (2010).
- 726 4. Jensen, R. E., & Englund, P. T. Network news: the replication of kinetoplast  
727 DNA. *Annu. Rev. Microbiol*. **66**, 473–491. [https://doi.org/10.1146/annurev-micro-](https://doi.org/10.1146/annurev-micro-092611-150057)  
728 [092611-150057](https://doi.org/10.1146/annurev-micro-092611-150057) (2012).
- 729 5. Ogbadoyi, E. O., Robinson, D. R. & Gull, K. A high-order trans-membrane structural  
730 linkage is responsible for mitochondrial genome positioning and segregation by  
731 flagellar basal bodies in trypanosomes. *Molecular biology of the cell*, **14**(5), 1769–  
732 1779. <https://doi.org/10.1091/mbc.e02-08-0525> (2003).
- 733 6. Tittawella I. Kinetoplast-associated proteins as potential drug targets and diagnostic  
734 markers for trypanosomiasis. *The Journal of infection*, **29**(3), 359–361.  
735 [https://doi.org/10.1016/s0163-4453\(94\)91496-6](https://doi.org/10.1016/s0163-4453(94)91496-6) (1994).
- 736 7. Mukherjee, S. *et al.* Metabolic Inhibitors as Antiparasitic Drugs: Pharmacological,  
737 Biochemical and Molecular Perspectives. *Current drug metabolism*, **17**(10), 937–  
738 970. <https://doi.org/10.2174/1389200217666161004143152> (2016).
- 739 8. Menna-Barreto, R. F. & de Castro, S. L. Clear Shot at Primary Aim: Susceptibility of  
740 *Trypanosoma cruzi* Organelles, Structures and Molecular Targets to Drug



- 741 Treatment. *Curr. Top. Med. Chem.* **17**(10), 1212–1234.  
742 <https://doi.org/10.2174/15680266166666161025161858> (2017).
- 743 9. Mensa-Wilmot, K. *et al.* Kinetoplast Division Factors in a Trypanosome. *Trends*  
744 *Parasitol.*, **35**(2), 119–128. <https://doi.org/10.1016/j.pt.2018.11.002> (2019).
- 745 10. De Souza W. Basic cell biology of *Trypanosoma cruzi*. *Curr. Pharm. Des.*, **8**(4), 269–  
746 285. <https://doi.org/10.2174/1381612023396276> (2002).
- 747 11. de Souza, S. *et al.* Expanded repertoire of kinetoplast associated proteins and unique  
748 mitochondrial DNA arrangement of symbiont-bearing trypanosomatids. *PLoS*  
749 *one*, **12**(11), e0187516. <https://doi.org/10.1371/journal.pone.0187516> (2017).
- 750 12. Gonçalves, C. S. *et al.* Revisiting the *Trypanosoma cruzi* metacyclogenesis:  
751 morphological and ultrastructural analyses during cell differentiation. *Parasit*  
752 *Vectors*, **11**(1), 83. <https://doi.org/10.1186/s13071-018-2664-4> (2018).
- 753 13. Xu, C. W. *et al.* Nucleus-encoded histone H1-like proteins are associated with  
754 kinetoplast DNA in the trypanosomatid *Crithidia fasciculata*. *Mol. Cell. Biol.*, **16**(2),  
755 564–576. <https://doi.org/10.1128/mcb.16.2.564> (1996).
- 756 14. Xu, C. & Ray, D. S. Isolation of proteins associated with kinetoplast DNA networks  
757 in vivo. *Proc Natl Acad Sci USA*, **90**(5), 1786–1789.  
758 <https://doi.org/10.1073/pnas.90.5.1786> (1993).
- 759 15. Lukes, J. *et al.* Disruption of the *Crithidia fasciculata* KAP1 gene results in structural  
760 rearrangement of the kinetoplast disc. *Mol Biochem Parasitol*, **117**(2), 179–186.  
761 [https://doi.org/10.1016/s0166-6851\(01\)00348-6](https://doi.org/10.1016/s0166-6851(01)00348-6) (2001).
- 762 16. Avliyakov, N. K., Lukes, J., & Ray, D. S. Mitochondrial histone-like DNA-binding  
763 proteins are essential for normal cell growth and mitochondrial function in *Crithidia*  
764 *fasciculata*. *Eukaryotic cell*, **3**(2), 518–526. [https://doi.org/10.1128/ec.3.2.518-](https://doi.org/10.1128/ec.3.2.518-526.2004)  
765 [526.2004](https://doi.org/10.1128/ec.3.2.518-526.2004) (2004).
- 766 17. Kapeller, I., Milman, N., Yaffe, N., & Shlomai, J. Interactions of a replication initiator  
767 with histone H1-like proteins remodel the condensed mitochondrial genome. *J. Biol.*  
768 *Chem.*, **286**(47), 40566–40574. <https://doi.org/10.1074/jbc.M111.270322> (2011).
- 769 18. Cavalcanti, D. P. *et al.* The effect of topoisomerase II inhibitors on the kinetoplast  
770 ultrastructure. *Parasitol. Res.* **94**(6), 439–448. [https://doi.org/10.1007/s00436-004-](https://doi.org/10.1007/s00436-004-1223-4)  
771 [1223-4](https://doi.org/10.1007/s00436-004-1223-4) (2004).
- 772 19. de Souza, F. S. *et al.* Knockout of the gene encoding the kinetoplast-associated protein  
773 3 (KAP3) in *Trypanosoma cruzi*: effect on kinetoplast organization, cell proliferation

- 774 and differentiation. *Mol Biochem Parasitol*, **172**(2), 90–98.  
775 <https://doi.org/10.1016/j.molbiopara.2010.03.014> (2010).
- 776 20. Wang, J., Pappas-Brown, V., Englund, P. T., & Jensen, R. E. TbKAP6, a  
777 mitochondrial HMG box-containing protein in *Trypanosoma brucei*, is the first  
778 trypanosomatid kinetoplast-associated protein essential for kinetoplast DNA  
779 replication and maintenance. *Eukaryotic cell*, **13**(7), 919–932.  
780 <https://doi.org/10.1128/EC.00260-13> (2014).
- 781 21. Teixeira, M.M *et al.* Phylogenetic validation of the genera *Angomonas* and  
782 *Strigomonas* of trypanosomatids harboring bacterial endosymbionts with the  
783 description of new species of trypanosomatids and of proteobacterial symbionts.  
784 *Protist*. **162**(3): 503-524. <https://doi.org/10.1016/j.protis.2011.01.001> (2011)
- 785 22. Motta, M. C. *et al.* The bacterium endosymbiont of *Crithidia deanei* undergoes  
786 coordinated division with the host cell nucleus. *PloS one*, **5**(8), e12415.  
787 <https://doi.org/10.1371/journal.pone.0012415> (2010).
- 788 23. Brum, F. L. *et al.* Structural characterization of the cell division cycle in *Strigomonas*  
789 *culicis*, an endosymbiont-bearing trypanosomatid. *Microsc Microanal.* **20**(1), 228–  
790 237. <https://doi.org/10.1017/S1431927613013925> (2014).
- 791 24. Catta-Preta, C. M. *et al.* Endosymbiosis in trypanosomatid protozoa: the bacterium  
792 division is controlled during the host cell cycle. *Front Microbiol*, **6**, 520.  
793 <https://doi.org/10.3389/fmicb.2015.00520> (2015).
- 794 25. Motta, M.C.M. *et al.* Detection of penicillin binding proteins in the endosymbiont of  
795 the trypanosomatid *Crithidia deanei*. *J. Eukaryotic Microbiol.* **44**: 492-496 (1997a).
- 796 26. Alves, J. M. *et al.* Genome evolution and phylogenomic analysis of Candidatus  
797 Kinetoplastibacterium, the betaproteobacterial endosymbionts of *Strigomonas* and  
798 *Angomonas*. *Genome Biol. Evol.* **5**(2), 338–350. <https://doi.org/10.1093/gbe/evt012>  
799 (2013).
- 800 27. Motta, M. C. *et al.* Predicting the proteins of *Angomonas deanei*, *Strigomonas culicis*  
801 and their respective endosymbionts reveals new aspects of the trypanosomatidae  
802 family. *PloS one*, **8**(4), e60209. <https://doi.org/10.1371/journal.pone.0060209>  
803 (2013).
- 804 28. Cavalcanti, D. P., Thiry, M., de Souza, W. & Motta, M. C. The kinetoplast  
805 ultrastructural organization of endosymbiont-bearing trypanosomatids as revealed by  
806 deep-etching, cytochemical and immunocytochemical analysis. *Histochem Cell*  
807 *Biol*, **130**(6), 1177–1185. <https://doi.org/10.1007/s00418-008-0450-7> (2008).

- 808 29. Zuma, A. A. *et al.* Effect of topoisomerase inhibitors and DNA-binding drugs on the  
809 cell proliferation and ultrastructure of *Trypanosoma cruzi*. *Int. J. Antimicrob.*, **37**(5),  
810 449–456. <https://doi.org/10.1016/j.ijantimicag.2010.11.031> (2011).
- 811 30. Chatterjee, A., & Singh, K. K. Uracil-DNA glycosylase-deficient yeast exhibit a  
812 mitochondrial mutator phenotype. *Nucleic acids research*, **29**(24), 4935–4940.  
813 <https://doi.org/10.1093/nar/29.24.4935> (2001).
- 814 31. Nakabeppu Y. Regulation of intracellular localization of human MTH1, OGG1, and  
815 MYH proteins for repair of oxidative DNA damage. *Progress in nucleic acid*  
816 *research and molecular biology*, **68**, 75–94. [https://doi.org/10.1016/s0079-](https://doi.org/10.1016/s0079-6603(01)68091-7)  
817 [6603\(01\)68091-7](https://doi.org/10.1016/s0079-6603(01)68091-7) (2001).
- 818 32. Takao, M., Zhang, Q. M., Yonei, S., & Yasui, A. Differential subcellular  
819 localization of human MutY homolog (hMYH) and the functional activity of  
820 adenine:8-oxoguanine DNA glycosylase. *Nucleic acids research*, **27**(18), 3638–  
821 3644. <https://doi.org/10.1093/nar/27.18.3638> (1999).
- 822 33. Han, D. *et al.* NEIL1 and NEIL2 DNA glycosylases protect neural crest  
823 development against mitochondrial oxidative stress. *eLife*, **8**, e49044.  
824 <https://doi.org/10.7554/eLife.49044> (2019).
- 825 34. Mitra, S., *et al.* Intracellular trafficking and regulation of mammalian AP-  
826 endonuclease 1 (APE1), an essential DNA repair protein. *DNA repair*, **6**(4), 461–  
827 469. <https://doi.org/10.1016/j.dnarep.2006.10.010> (2007).
- 828 35. Tsuchimoto, D. *et al.* Human APE2 protein is mostly localized in the nuclei and to  
829 some extent in the mitochondria, while nuclear APE2 is partly associated with  
830 proliferating cell nuclear antigen. *Nucleic Acids Res*, **29**(11), 2349–2360.  
831 <https://doi.org/10.1093/nar/29.11.2349> (2001)
- 832 36. Kalifa, L., Beutner, G., Phadnis, N., Sheu, S. S., & Sia, E. A. Evidence for a role of  
833 FEN1 in maintaining mitochondrial DNA integrity. *DNA repair*, **8**(10), 1242–1249.  
834 <https://doi.org/10.1016/j.dnarep.2009.07.008> (2009).
- 835 37. Kazak, L. *et al.* A cryptic targeting signal creates a mitochondrial FEN1 isoform  
836 with tailed R-Loop binding properties. *PloS one*, **8**(5), e62340.  
837 <https://doi.org/10.1371/journal.pone.0062340> (2013).
- 838 38. Zheng, L. *et al.* Human DNA2 is a mitochondrial nuclease/helicase for efficient  
839 processing of DNA replication and repair intermediates. *Molecular cell*, **32**(3), 325–  
840 336. <https://doi.org/10.1016/j.molcel.2008.09.024> (2008).

- 841 39. Mason, P. A., Matheson, E. C., Hall, A. G., & Lightowers, R. N. Mismatch repair  
842 activity in mammalian mitochondria. *Nucleic Acids Res*, **31**(3), 1052–1058.  
843 [https://doi.org/10.1093/nar/gkg167\(2003\)](https://doi.org/10.1093/nar/gkg167(2003)).
- 844 40. Clayton, D. A., Doda, J. N., & Friedberg, E. C. The absence of a pyrimidine dimer  
845 repair mechanism in mammalian mitochondria. *Proc Natl Acad Sci USA*, **71**(7),  
846 2777–2781. <https://doi.org/10.1073/pnas.71.7.2777> (1974).
- 847 41. Podratz, J. L. *et al.* Cisplatin induced mitochondrial DNA damage in dorsal root  
848 ganglion neurons. *Neurobiol. Dis.*, **41**(3), 661–668.  
849 <https://doi.org/10.1016/j.nbd.2010.11.017> (2011).
- 850 42. Pascucci, B. *et al.* DNA repair of UV photoproducts and mutagenesis in human  
851 mitochondrial DNA. *J. Mol. Biol.*, **273**(2), 417–427.  
852 <https://doi.org/10.1006/jmbi.1997.1268> (1997).
- 853 43. Furtado, C. *et al.* Functional characterization of 8-oxoguanine DNA glycosylase of  
854 *Trypanosoma cruzi*. *PLoS one*, **7**(8), e42484.  
855 <https://doi.org/10.1371/journal.pone.0042484> (2012).
- 856 44. Kunrath-Lima, M. *et al.* Characterization of *Trypanosoma cruzi* MutY DNA  
857 glycosylase ortholog and its role in oxidative stress response. *Infect. Genet. Evol.*  
858 **55**, 332–342 <https://doi.org/10.1016/j.meegid.2017.09.030> (2017).
- 859 45. Aguiar, P. H. N. *et al.* Oxidative stress and DNA lesions: the role of 8-oxoguanine  
860 lesions in *Trypanosoma cruzi* cell viability. *PLoS Negl. Trop. Dis.*, **7**(6), e2279.  
861 <https://doi.org/10.1371/journal.pntd.0002279> (2013).
- 862 46. Lopes, D. de O. *et al.* Biochemical studies with DNA polymerase  $\beta$  and DNA  
863 polymerase  $\beta$ -PAK of *Trypanosoma cruzi* suggest the involvement of these proteins  
864 in mitochondrial DNA maintenance. *DNA Repair (Amst)*, **7**(11), 1882–1892.  
865 <https://doi.org/10.1016/j.dnarep.2008.07.018> (2008).
- 866 47. Schamber-Reis, B. L. F. *et al.* DNA polymerase beta from *Trypanosoma cruzi* is  
867 involved in kinetoplast DNA replication and repair of oxidative lesions. *Mol.*  
868 *Biochem. Parasitol.*, **183**(2), 122–131.  
869 <https://doi.org/10.1016/j.molbiopara.2012.02.007> (2012).
- 870 48. Rajão, M. A. *et al.* DNA polymerase kappa from *Trypanosoma cruzi* localizes to the  
871 mitochondria, bypasses 8-oxoguanine lesions and performs DNA synthesis in a  
872 recombination intermediate. *Mol. Microbiol.*, **71**(1), 185–197.  
873 <https://doi.org/10.1111/j.1365-2958.2008.06521.x> (2009).

- 874 49. Vieira-da-Rocha, J. P. *et al.* The DNA damage response is developmentally  
875 regulated in the African trypanosome. *DNA Repair* (Amst). **73**, 78–90  
876 <https://doi.org/10.1016/j.dnarep.2018.11.005> (2018).
- 877 50. Warren L. G. Metabolism of *Schizotrypanum cruzi* Chagas. I. Effect of culture age  
878 and substrate concentration on respiratory rate. *The Journal of parasitology*, **46**,  
879 529–539 (1960).
- 880 51. Beneke, T. *et al.* A CRISPR Cas9 high-throughput genome editing toolkit for  
881 kinetoplastids. *Royal Society open science*, **4**(5), 170095.  
882 <https://doi.org/10.1098/rsos.170095> (2017).
- 883 52. Peng, D., & Tarleton, R. EuPaGDT: a web tool tailored to design CRISPR guide  
884 RNAs for eukaryotic pathogens. *Microbial genomics*, **1**(4), e000033.  
885 <https://doi.org/10.1099/mgen.0.000033> (2015).
- 886 53. Davey, J. W. *et al.* Chromosomal assembly of the nuclear genome of the  
887 endosymbiont-bearing trypanosomatid *Angomonas deanei*. *G3* (Bethesda,  
888 Md.), **11**(1), jkaa018. <https://doi.org/10.1093/g3journal/jkaa018> (2021).
- 889 54. Andrade, I. d. S., *et al.* Characterization of a porin channel in the endosymbiont of  
890 the trypanosomatid protozoan *Crithidia deanei*. *Microbiology*, **157**(10), 2818–  
891 2830. <https://doi.org/10.1099/mic.0.049247-0> (2011)
- 892 55. Liu, Y., & Englund, P. T. The rotational dynamics of kinetoplast DNA replication.  
893 *Mol. Microbiol.*, **64**(3), 676–690. doi:10.1111/j.1365-2958.2007.05686.x (2007).
- 894 56. Santos, J.H., Meyer, J.N., Mandavilli, B.S. and Van Houten, B. Quantitative PCR-  
895 based measurement of nuclear and mitochondrial DNA damage and repair in  
896 mammalian cells. *Methods Mol. Biol.* 7:183. <https://doi:10.1385/1-59259-973-7:183>  
897 (2006).
- 898 57. Huang, H., Zhu, L., Reid, B. R., Drobny, G. P., & Hopkins, P. B. Solution structure  
899 of a cisplatin-induced DNA interstrand cross-link. *Science* **270** (5243), 1842–1845.  
900 <https://doi.org/10.1126/science.270.5243.1842> (1995).
- 901 58. Ohndorf, U. M., Rould, M. A., He, Q., Pabo, C. O., & Lippard, S. J. Basis for  
902 recognition of cisplatin-modified DNA by high-mobility-group  
903 proteins. *Nature*, **399** (6737), 708–712. <https://doi.org/10.1038/21460> (1999).
- 904 59. Siddik, Z. H. Cisplatin: Mode of cytotoxic action and molecular basis of resistance.  
905 *Oncogene* **22** 7265–7279. <https://doi:10.1038/sj.onc.1206933> (2003).

- 906 60. Alt, A. *et al.* Bypass of DNA lesions generated during anticancer treatment with  
907 cisplatin by DNA polymerase *eta*. *Science*, **318**(5852), 967–970.  
908 <https://doi.org/10.1126/science.1148242> (2007).
- 909 61. Todd, R. C., & Lippard, S. J. Inhibition of transcription by platinum antitumor  
910 compounds. *Metallomics : integrated biometal science*, **1**(4), 280–291.  
911 <https://doi.org/10.1039/b907567d> (2009).
- 912 62. Morales, J., *et al.* Development of a toolbox to dissect host-endosymbiont  
913 interactions and protein trafficking in the trypanosomatid *Angomonas*  
914 *deanei*. *BMC Evol Biol*, **16**(1), 247. <https://doi.org/10.1186/s12862-016-0820-z>  
915 (2016).
- 916 63. Beneke, T., *et al.* Genetic dissection of a *Leishmania* flagellar proteome  
917 demonstrates requirement for directional motility in sand fly infections. *PLoS*  
918 *pathogens*, **15**(6), e1007828. <https://doi.org/10.1371/journal.ppat.1007828> (2019)
- 919 64. Soares Medeiros, L. C. *et al.* Rapid, Selection-Free, High-Efficiency Genome  
920 Editing in Protozoan Parasites Using CRISPR-Cas9  
921 Ribonucleoproteins. *mBio*, **8**(6), e01788-17. [https://doi.org/10.1128/mBio.01788-  
922 17](https://doi.org/10.1128/mBio.01788-17) (2017).
- 923 65. Beck, K. *et al.* *Trypanosoma brucei* Tb927.2.6100 is an essential protein associated  
924 with kinetoplast DNA. *Eukaryotic cell*, **12**(7), 970–978.  
925 <https://doi.org/10.1128/EC.00352-12> (2013).
- 926 66. Hammarton T. C. Cell cycle regulation in *Trypanosoma brucei*. *Mol Biochem*  
927 *Parasitol*, **153**(1), 1–8. <https://doi.org/10.1016/j.molbiopara.2007.01.017> (2007).
- 928 67. Jones, N. G. *et al.* Regulators of *Trypanosoma brucei* cell cycle progression and  
929 differentiation identified using a kinome-wide RNAi screen. *PLoS*  
930 *pathogens*, **10**(1), e1003886. <https://doi.org/10.1371/journal.ppat.1003886> (2014).
- 931 68. Pasternack, D. A., *et al.* Sphingosine Kinase Regulates Microtubule Dynamics and  
932 Organelle Positioning Necessary for Proper G1/S Cell Cycle Transition in  
933 *Trypanosoma brucei*. *mBio*, **6**(5), e01291-15. [https://doi.org/10.1128/mBio.01291-  
934 15](https://doi.org/10.1128/mBio.01291-15) (2015).
- 935 69. Benz, C., & Urbaniak, M. D. Organising the cell cycle in the absence of  
936 transcriptional control: Dynamic phosphorylation co-ordinates the *Trypanosoma*  
937 *brucei* cell cycle post-transcriptionally. *PLoS pathogens*, **15**(12), e1008129.  
938 <https://doi.org/10.1371/journal.ppat.1008129> (2019).

- 939 70. Klebanov-Akopyan, O. *et al.* *Trypanosoma brucei* UMSBP2 is a single-stranded  
940 telomeric DNA binding protein essential for chromosome end protection. *Nucleic*  
941 *acids research*, **46**(15), 7757–7771. <https://doi.org/10.1093/nar/gky597> (2018).
- 942 71. Li, Y., Sun, Y., Hines, J. C., & Ray, D. S. Identification of new kinetoplast DNA  
943 replication proteins in trypanosomatids based on predicted S-phase expression and  
944 mitochondrial targeting. *Eukaryotic cell*, **6**(12), 2303–2310.  
945 <https://doi.org/10.1128/EC.00284-07> (2007).
- 946 72. Amodeo, S., Jakob, M., & Ochsenreiter, T. Characterization of the novel  
947 mitochondrial genome replication factor MiRF172 in *Trypanosoma brucei*. *Journal*  
948 *of cell science*, **131**(8), jcs211730. <https://doi.org/10.1242/jcs.211730> (2018).
- 949 73. Týč, J., Klingbeil, M. M., & Lukeš, J. Mitochondrial heat shock protein machinery  
950 hsp70/hsp40 is indispensable for proper mitochondrial DNA maintenance and  
951 replication. *mBio*, **6**(1), e02425-14. <https://doi.org/10.1128/mBio.02425-14> (2015).
- 952 74. Brueckner, F., Hennecke, U., Carell, T., & Cramer, P. CPD damage recognition by  
953 transcribing RNA polymerase II. *Science*, **315**(5813), 859–862.  
954 <https://doi.org/10.1126/science.1135400> (2007).
- 955 75. Hanawalt, P. C., & Spivak, G. Transcription-coupled DNA repair: two decades of  
956 progress and surprises. *Nature reviews. Molecular cell biology*, **9**(12), 958–970.  
957 <https://doi.org/10.1038/nrm2549> (2008).
- 958 76. McCulloch, R., & Barry, J. D. A role for RAD51 and homologous recombination in  
959 *Trypanosoma brucei* antigenic variation. *Genes & development*, **13**(21), 2875–  
960 2888. <https://doi.org/10.1101/gad.13.21.2875> (1999).
- 961 77. Dobson, R. *et al.* Interactions among *Trypanosoma brucei* RAD51 paralogues in  
962 DNA repair and antigenic variation. *Molecular microbiology*, **81**(2), 434–456.  
963 <https://doi.org/10.1111/j.1365-2958.2011.07703.x> (2011).
- 964 78. Grazielle-Silva, V. *et al.* *Trypanosoma brucei* and *Trypanosoma cruzi* DNA  
965 Mismatch Repair Proteins Act Differently in the Response to DNA Damage Caused  
966 by Oxidative Stress. *Front Cell Infect Microbiol*, **10**, 154.  
967 <https://doi.org/10.3389/fcimb.2020.00154> (2020).

968

## 969 **Acknowledgement**

970 This work was supported by CNPq and FAPERJ. JCM is supported by the Wellcome  
971 Trust (200807/Z/16/Z).

972

### 973 **Author Contributions**

974 Conceived and designed the experiments: MCMM CRM CMCC-P. Acquisition of data:  
975 CSG CMCC-P BR Analyzed the data: MCMM CRM CSG CMCC-P BR JCM WS  
976 Contributed reagents/materials: MCMM CRM JCM WS. Wrote the paper: MCMM CRM  
977 CMCC-P CSG BR. Revised the paper: CSG CMCC-P BR WS JCM CRM MCMM

978

### 979 **Figure Legends**

980

981 **Figure 1:** Generation of *KAP4* mutants, cell proliferation and viability. qPCR  
982 amplification showing that there was no damage to the nuclear (a) and mitochondrial (b)  
983 DNA of the T7RNAPol-SpCas9 cells compared to WT cells. (c) Diagram representing  
984 the sgRNA PCR transfection that allows for double strand breaks (DSBs) at the 5' and 3'  
985 ends of the genes and repair-templates mediated recombination at the UTRs 30 nt  
986 upstream and downstream of the CDS. Diagnostic PCR oligonucleotides were designed  
987 to amplify the integrated NEO repair template, binding upstream of the open reading  
988 frame (OL5) and internally to the NEO gene (OL6), and the presence (WT and +/-) or  
989 absence (-/-) of *KAP4* (650 bp, OL5+OL7). (d) Diagnostic PCR showing *KAP4* gene  
990 deletion and Neo selectable marker integration in the *A. deanei* genome. (e) Growth curve  
991 for 72 h showed that *KAP4* mutants present a reduced proliferation in relation to WT and  
992 T7RNAPol-SpCas9 strains. Cell number was plotted on a logarithmic scale, and the  
993 presented data are the mean  $\pm$  s.d. of three independent cell cultures. After 48 h, when  
994 cells reached the peak of the exponential phase, a paired T test ( $p < 0.05$ ) was performed  
995 to compare control and mutant cells. (f) Duplication time of WT, T7RNAPol-SpCas9 and  
996 cells deleted for *KAP4*. (g) The cell viability was similar among the strains analyzed and  
997 maintained even after 72 h of cultivation. The presented data is a mean  $\pm$  s.d. of three  
998 independent cell cultures. WT, wild-type cells, *kap4*<sup>+/-</sup>, cells with deletion for one allele,  
999 *kap4*<sup>-/-</sup>, null mutant.

1000

1001 **Figure 2:** Ultrastructure and morphology of *A. deanei*. WT (a-c), T7RNAPol-SpCas9 (d-  
1002 f) and *KAP4* mutant cells with single (g-l) or double deletions (m-r). (a-b) Transmission



1003 electron microscopy of WT cells showed typical characteristics of symbiont-harboring  
1004 trypanosomatids, which were also observed in T7RNAPol-SpCas9 cells (**d-e**). *kap4*<sup>+/-</sup> and  
1005 *kap4*<sup>-/-</sup> cells presented ultrastructural alterations as a high condensation of nuclear DNA  
1006 (**g**), a densely packed kDNA (**i-o**), a filamentous symbiont (**h, n**), dividing cells with two  
1007 flagella in the same flagellar pocket (**m**). Scanning electron microscopy showed the  
1008 typical choanomastigote form in WT and T7RNAPol-SpCas9 cells of mutant cells (**c** and  
1009 **f**). *kap4*<sup>+/-</sup> mutants presented ultrastructure alterations such as asymmetric division (**j**,  
1010 yellow arrow), which generated cells with different dimensions (**k**) and protozoa with  
1011 multiple cell bodies and flagella (**l**). *kap4*<sup>-/-</sup> cells presented cytokinesis impairment that  
1012 generated a popcorn-like phenotype (**q-r**). In both mutant strains, cell bodies and  
1013 flagellum shortening were observed (**j** and **p**, white arrows). ht – heterochromatin, k-  
1014 kinetoplast, lb - lipid body, n - nucleus, nu - nucleolus, s - symbiont, f – flagellum, fs -  
1015 filamentous symbiont, v - vacuole. Brackets show the more densely packed kDNA.

1016

1017 **Figure 3:** Atypical phenotypes were observed in *KAP4* mutant cells cultivated for 24 h  
1018 after labeling with DAPI and anti-porin antibodies. WT (**a-a''**); *kap4*<sup>+/-</sup> mutants containing  
1019 one filamentous symbiont with multiple nucleoids (Fs - green arrowhead), one nucleus  
1020 (N-white arrows) and one kinetoplast (K-white arrowhead) (**b-b''**) or two nuclei and two  
1021 kinetoplasts and (**c-c''**); *kap4*<sup>-/-</sup> cells were seen with one filamentous symbiont, two nuclei  
1022 and one kinetoplast (**d-d''**). Bars 5  $\mu\text{m}$ . (**e**) Counting of cellular patterns showing that  
1023 filamentous symbionts (Fs) are more frequent in *kap4*<sup>-/-</sup>. (**f**) Percentage of cells presenting  
1024 atypical phenotypes. (**g**) *In situ* labeling showing the different stages of kDNA network  
1025 replication in WT and mutant cells (according to Liu and Englund 2007)<sup>15</sup>. Green  
1026 arrowheads indicate the symbiont, white arrows the nucleus and white arrowheads the  
1027 kinetoplast. Bars 1  $\mu\text{m}$ . t test p-value < 0.005. A total of 1,000 WT and *KAP4* mutant  
1028 cells were counted in 3 independent experiments.

1029

1030 **Figure 4:** Cell growth and survival after cisplatin treatment or UV radiation. After 12 h,  
1031 no remarkable differences were observed in cell proliferation and survival when  
1032 comparing WT and mutant protozoa after treatment with 150  $\mu\text{M}$  and 300  $\mu\text{M}$  cisplatin  
1033 (**a-b**) or exposure to UV radiation (**c-d**).

1034

1035 **Figure 5:** Effects of cisplatin on the ultrastructure of mutant cells as revealed by TEM (**a-**  
1036 **c, f-h, k-m**) and SEM (**d-e, i-j, n-o**). A-E: WT cells treated with cisplatin did not present  
1037 ultrastructural alterations by TEM. However, SEM showed rounded cells with a  
1038 shortening flagellum (**d-e**). (**f-o**) mutant cells treated with cisplatin. (**f**) Note DNA  
1039 unpacking in the nucleus (n), the proximity between the ER (black arrowhead) and the  
1040 endosymbiont, and mitochondrial branch swelling (m). (**g, l**) The symbiotic bacterium  
1041 presents alterations in the nuclear matrix and DNA condensation (white arrows). (**k-l**):  
1042 The symbiont presented membrane convolutions (black arrow) and was surrounded by  
1043 vacuoles, an indication of autophagy. (**h, m**) In mutant cells, the kDNA arrangement was  
1044 not affected in relation to protozoa not submitted to cisplatin treatment. n - nucleus, k -  
1045 kinetoplast, m - mitochondrial branch, s - symbiont, v - vacuole. (**d-e, i-j, n-o**) WT and  
1046 mutant cells of both types treated with cisplatin presented a rounded format containing a  
1047 shortening flagellum. Other atypical phenotypes, such as fat-cell shape (**d**), lack of  
1048 flagellum (**i** and **n**, arrowheads) and plasma membrane blebs (**o**, arrows), were also  
1049 observed.

1050

1051 **Figure 6:** DAPI-stained mutant protozoa presented different atypical phenotypes when  
1052 compared to WT cells after treatment with cisplatin for over 24 h (**a-c**). (**a-a''**) WT cells  
1053 treated with 150  $\mu$ M cisplatin presented rounded shapes, and the fat cell phenotype  
1054 contained a symbiont with multiple nucleoids (white square, green arrowheads). (**b-b''**)  
1055 Ad kap4<sup>(+/-)</sup> cells treated with 300  $\mu$ M cisplatin lacking the symbiont. (**c-c''**) Ad kap4<sup>(-/-)</sup>  
1056 cells treated with 300  $\mu$ M cisplatin containing one filamentous symbiont, two nuclei and  
1057 one kinetoplast. (**d**) Counting of cellular patterns considering the presence of normal or  
1058 filamentous symbionts. (**e**) Percentage of cells with atypical phenotypes. Bars 5  $\mu$ m. Fs -  
1059 Filamentous symbiont.; N- nucleus - white arrows; K-kinetoplast - white arrowheads. A  
1060 total of 1,000 cells of WT and KAP4 mutant cells were counted in 3 independent  
1061 experiments.

1062

1063 **Figure 7:** Effects of UV irradiation on the ultrastructure of WT and mutant cells as  
1064 revealed by TEM (**a-b, f-g, k-l**) and SEM (**c-e, h-j, m-o**). (**a-b**) WT cells submitted to  
1065 irradiation. Nuclear DNA condensation and kDNA arrangement were not modified.  
1066 However, the symbiont genome became densely packed (**a**, arrows). (**f-g, k-l**) mutant

1067 cells submitted to UV irradiation. Nuclear DNA condensation and kDNA arrangement  
1068 were not affected. **(f, k, g)** The symbiont was seen in association with the ER (white  
1069 arrowheads), and its DNA suffered condensation (white arrows). **(l)**  $kap4^{-/-}$  cells  
1070 containing multiple nuclei were also observed. fp - flagellar pocket, g - glycosome, k -  
1071 kinetoplast, m - mitochondrion, n - nucleus, s - symbiont. **(a-c)** WT cells subjected to  
1072 irradiation presented atypical formats indicating cytokinesis impairment. **(h-j)**  $kap4^{+/+}$   
1073 cells submitted to UV irradiation presented multiple interconnected cell bodies, indicating  
1074 that in such mutants, cytokinesis impairment was exacerbated in relation to WT protozoa.  
1075 **(m-o)**  $kap4^{-/-}$  cells submitted to UV irradiation presented a round cell body, and the  
1076 flagellum was short or even absent (white arrows).

1077

1078 **Figure 8:** DAPI-stained protozoa exposed to UV irradiation presented atypical  
1079 phenotypes. Such morphotypes were observed in WT cells **(a-a'')**, as well as in  $kap4^{+/+}$   
1080 **(b-b'')** and  $kap4^{-/-}$  **(c-c'')** mutant cells. **(a-a'')** Protozoa harboring two symbionts, two  
1081 nuclei, and one kinetoplast. **(b-b'')** A dyskinetoplastic protozoan, with a filamentous  
1082 symbiont containing multiple nucleoids and one nucleus. **(c-c'')** A cured cell containing  
1083 one nucleus and one kinetoplast. **(d)** Counting of cellular patterns considering the  
1084 presence of normal or filamentous symbionts, as well as cured cells (that lost the  
1085 symbiont) or lysed symbionts. **(e)** Percentage of cells presenting atypical phenotypes. S-  
1086 Symbiont and Fs - Filamentous symbiont, green arrowheads indicate bacterium  
1087 nucleoids; N- nucleus - white arrows; K-kinetoplast - white arrowhead. Bars 5  $\mu$ m. A  
1088 total of 1,000 WT and KAP4 mutant cells were counted in 3 independent experiments.

1089

1090 **Figure 9:** DNA repair kinetics of WT and mutant cells. **(a-b)** DNA repair kinetics of WT  
1091 cells compared to  $kap4^{+/+}$  cells (left panel) and  $kap4^{-/-}$  (right panel) after treatment with  
1092 300  $\mu$ M cisplatin. **(c-d)** DNA repair kinetics of WT cells in relation to  $kap4^{+/+}$  cells (left  
1093 panel) and  $kap4^{-/-}$  (right panel) after UV damage radiation. As observed for cisplatin, no  
1094 significant difference was observed in the DNA repair kinetics of all cell types.

1095

1096 **Table 1:** List of oligonucleotides for CRISPR-Cas9 in *A. deanei*, including sgRNA,  
1097 repair template and diagnostic PCR. Sequences are written in the 5' to 3' orientation.

1098

1099 **Supplementary Material 1:** Total protein extract of WT and T7RNAPol-SpCas9 mutant  
1100 strains of *A. deanei* and *L. mexicana*, here used as a control, were probed with anti-FLAG  
1101 antibody (Anti-FLAG M2, Sigma F3165; dilution 1:20,000) for detection of SpCas9 or  
1102 anti- $\beta$ -tubulin (Anti- $\beta$ -Tubulin clone AA2, Sigma T8328; dilution 1:10,000) used as  
1103 loading control.

1104

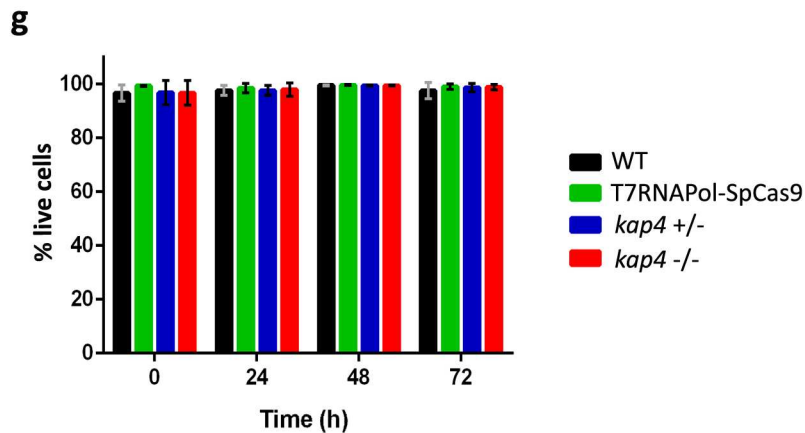
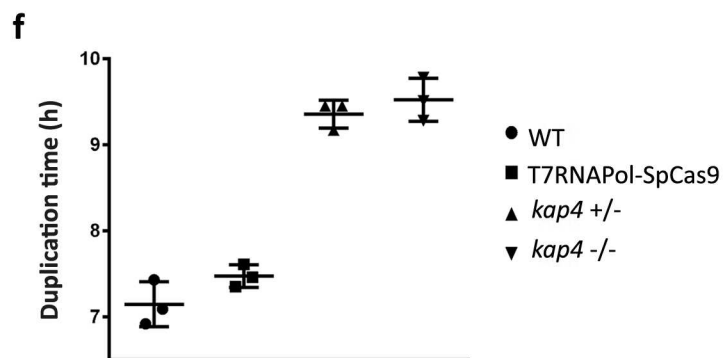
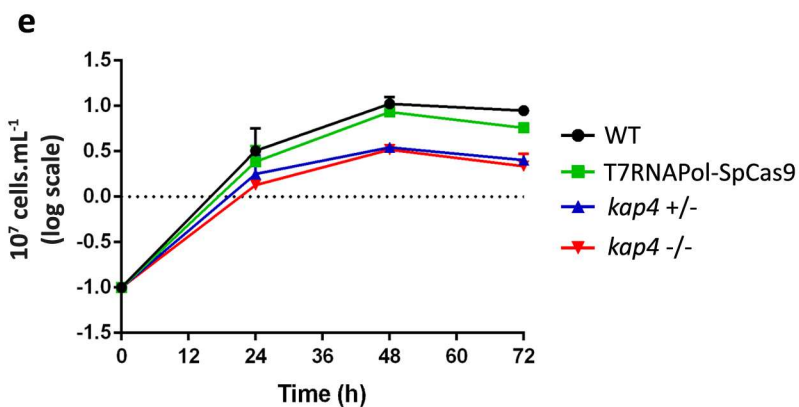
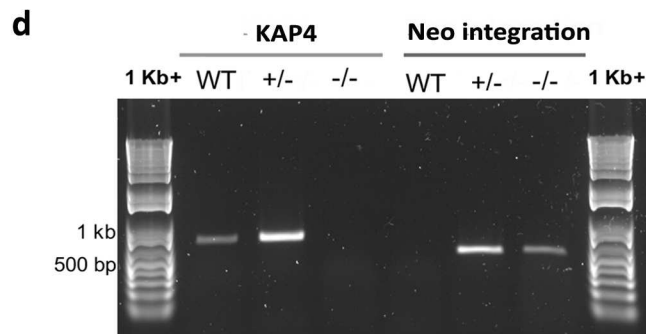
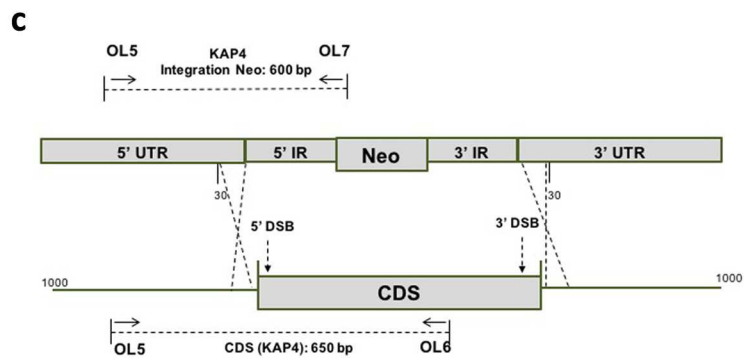
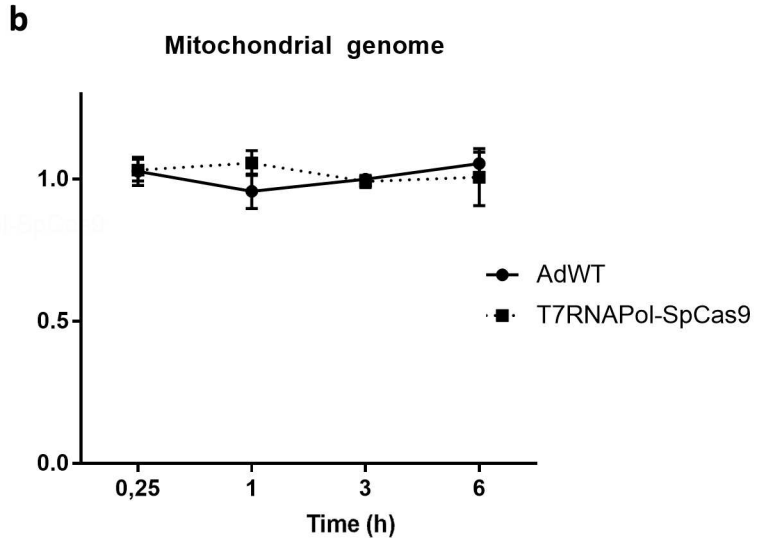
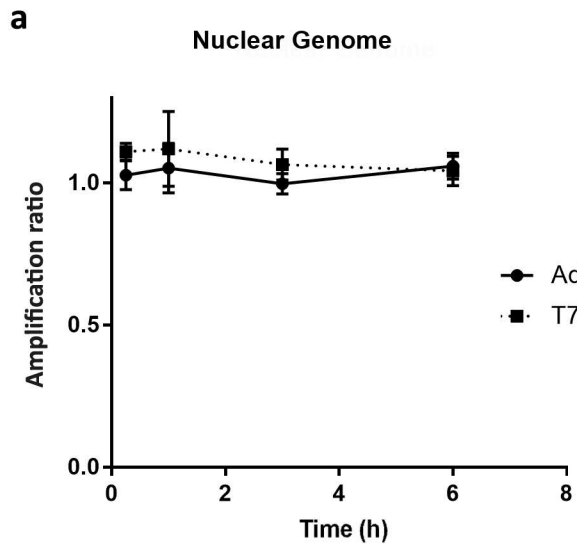
1105 **Supplementary Material 2:** Flow cytometry analysis of *A. deanei* DNA content in wild  
1106 type (WT) and mutant cells treated or not with cisplatin for 1 h or 24 h.

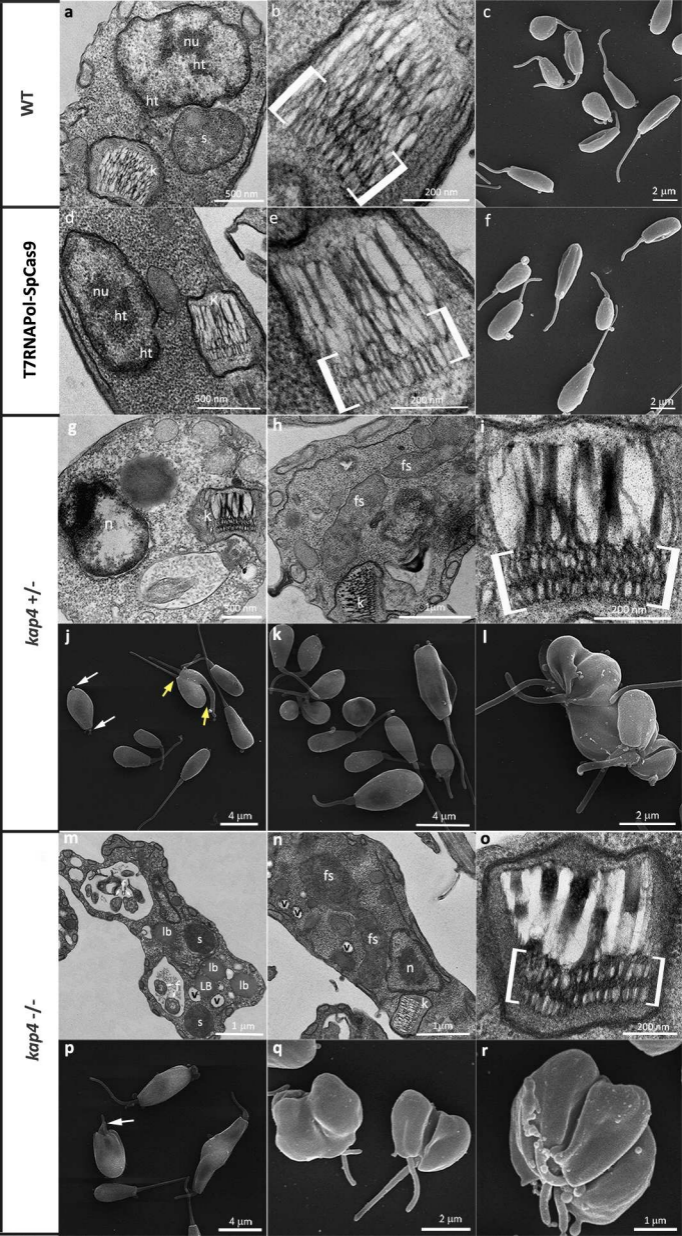
1107

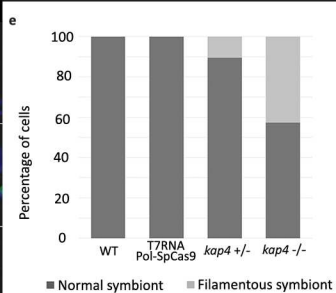
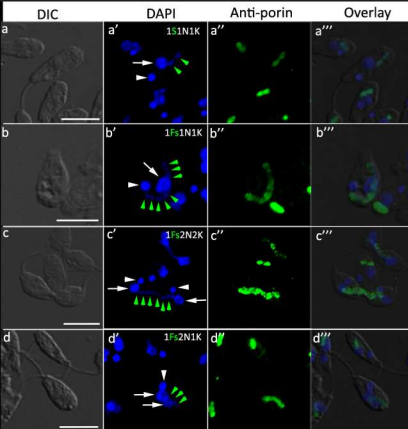
1108 **Supplementary Material 3:** DNA repair kinetics (0.25-6 h) measured by long-range  
1109 qPCR. Absorbance values for the smaller fragments of *A. deanei* WT, *kap4*<sup>+/-</sup> and *kap4*<sup>-/-</sup>

1110 .

1111

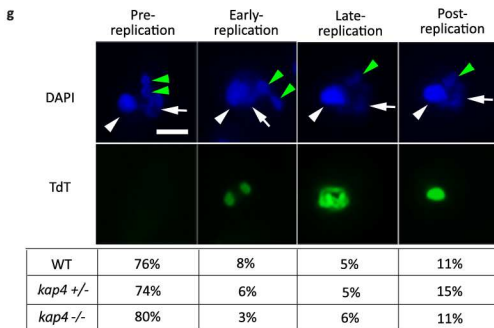






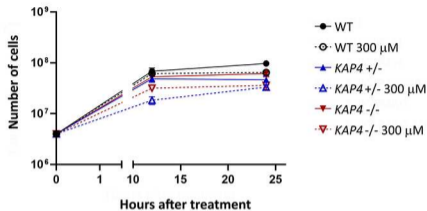
**f**

Atypical phenotypes	WT	T7RNAPol-SpCas9	<i>kap4 +/-</i>	<i>kap4 -/-</i>
1Fs1N1K	0,0%	0,0%	9,0%	39,3%
1Fs1N2K	0,0%	0,0%	0,0%	1,1%
1Fs2N2K	0,0%	0,0%	0,8%	0,0%
1Fs2N1K	0,0%	0,0%	0,8%	2,2%

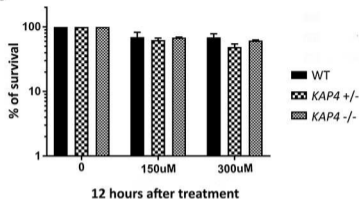


## Cisplatin treatment

a

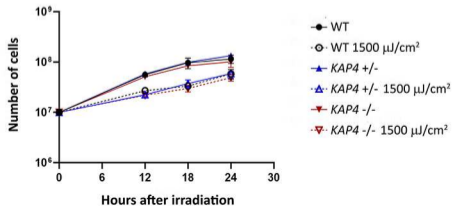


b

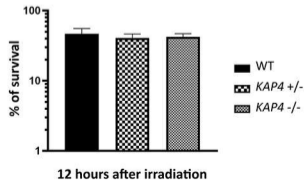


## Ultraviolet radiation

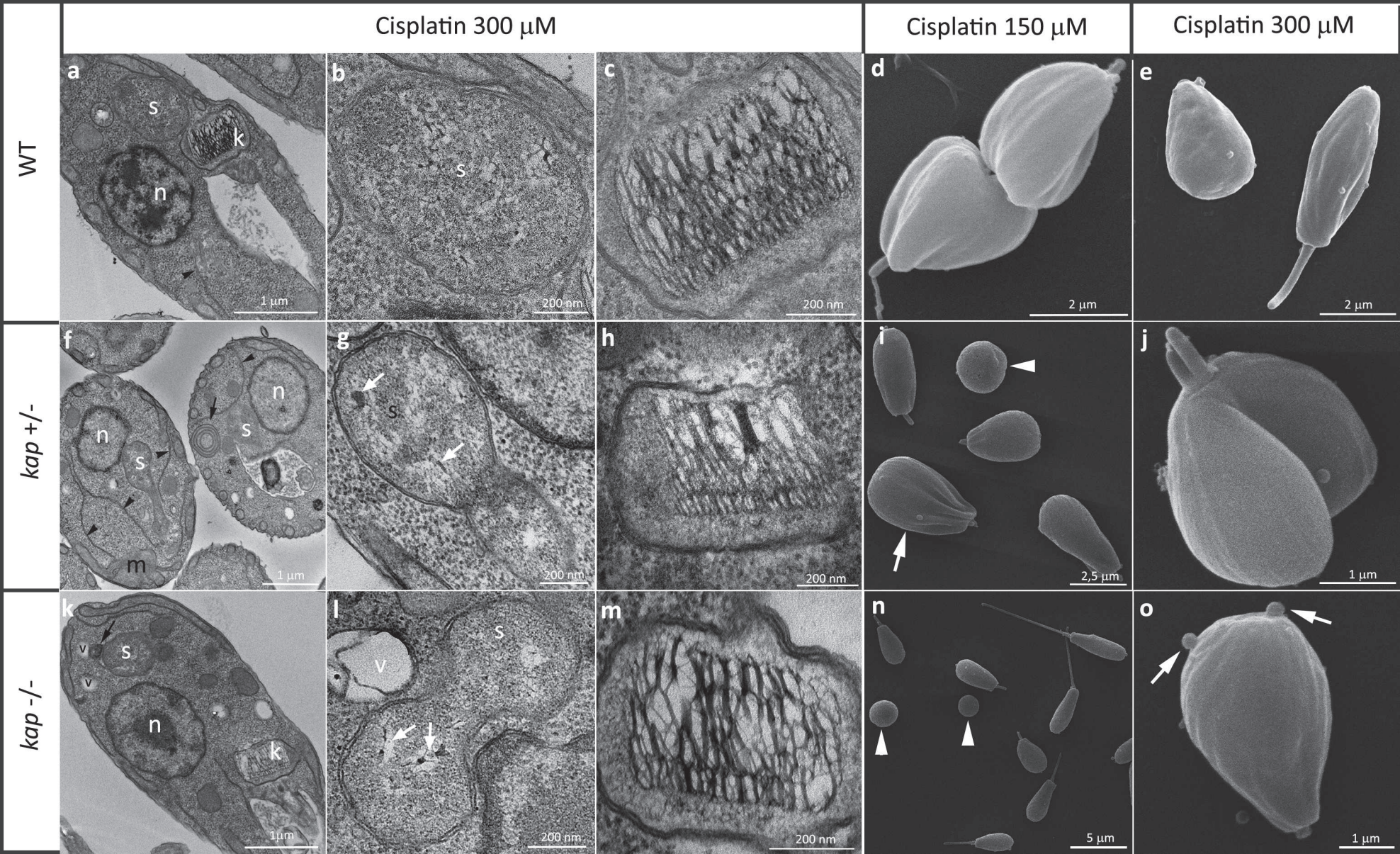
c

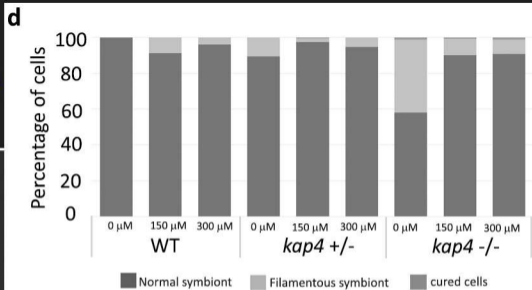
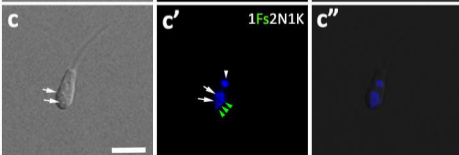
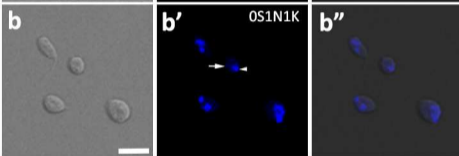
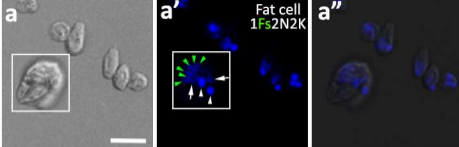


d





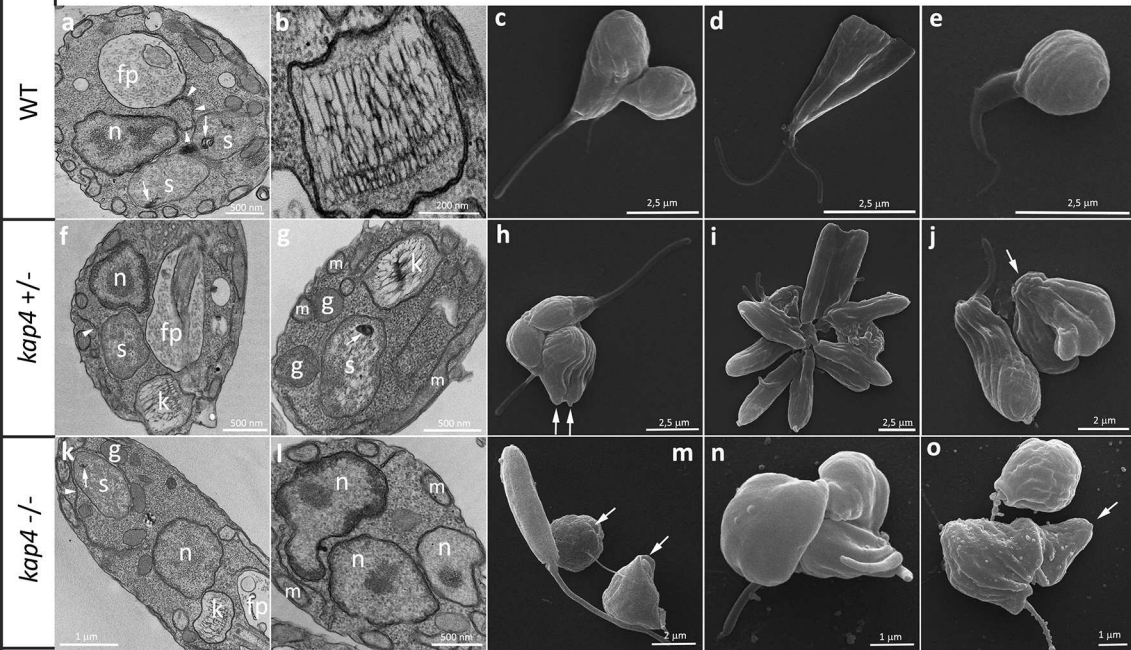


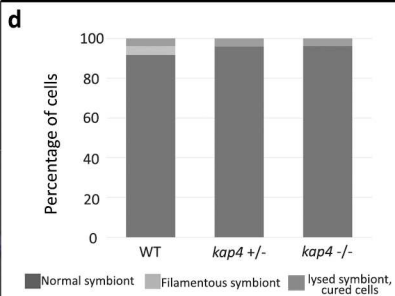
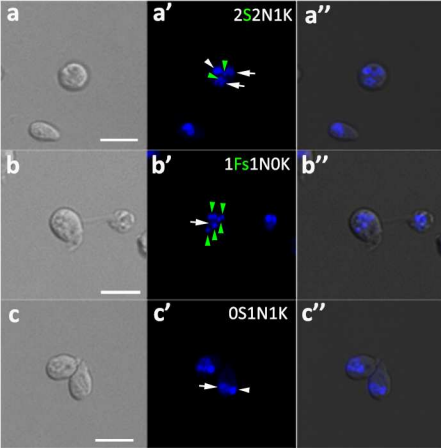


**e**

Atypical phenotypes	WT			<i>kap4 +/-</i>			<i>kap4 -/-</i>		
	0 $\mu$ M	150 $\mu$ M	300 $\mu$ M	0 $\mu$ M	150 $\mu$ M	300 $\mu$ M	0 $\mu$ M	150 $\mu$ M	300 $\mu$ M
1Fs1N1K	0,0%	7,8%	4,0%	9,0%	1,9%	5,3%	39,8%	9,2%	7,7%
1Fs2N2K	0,0%	1,0%	0,0%	0,8%	0,0%	0,0%	0,0%	0,0%	0,0%
1Fs2N1K	0,0%	0,0%	0,0%	0,8%	0,0%	0,0%	1,1%	0,0%	0,4%
OS1N1K	0,0%	0,0%	0,0%	0,0%	0,6%	0,0%	1,1%	0,8%	1,2%

UV radiation 1500  $\mu\text{J}/\text{cm}^2$

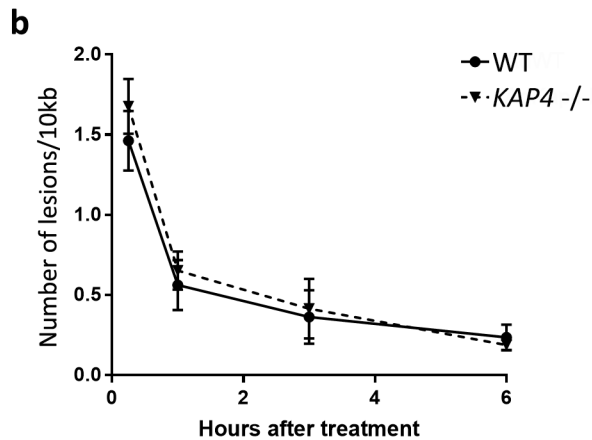
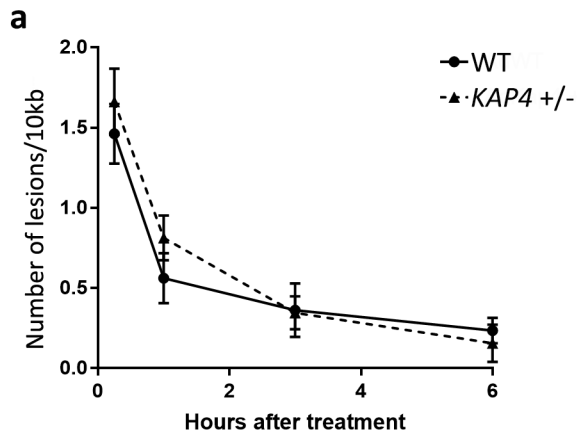




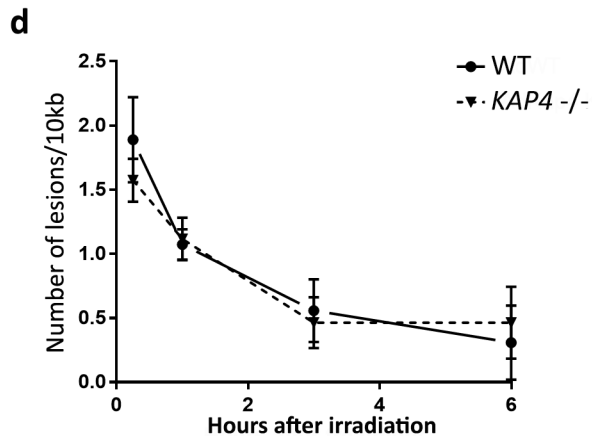
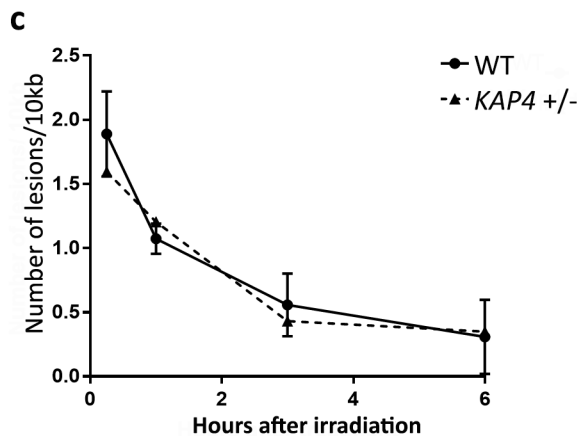
**e**

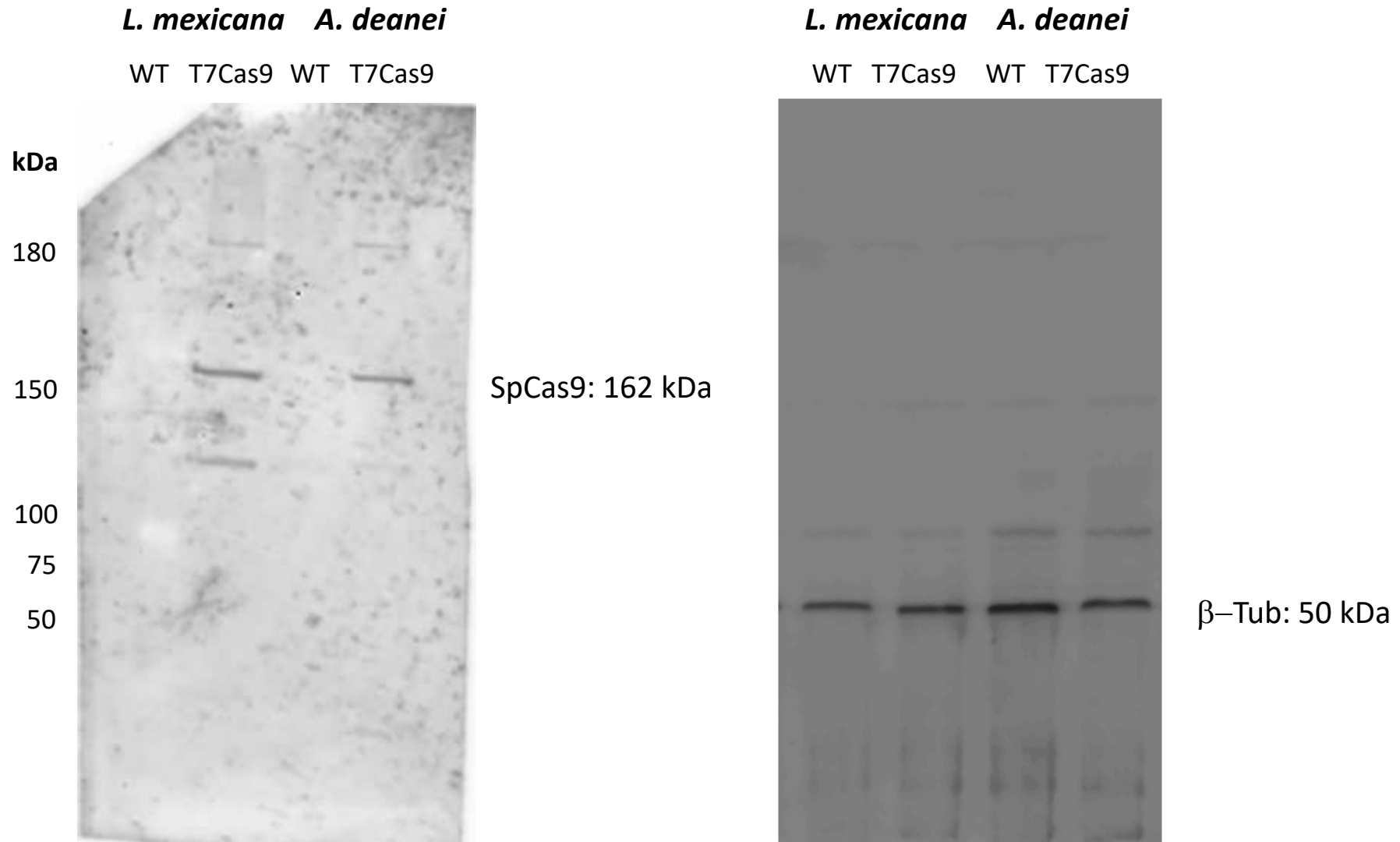
Atypical phenotypes	WT	<i>kap4 +/-</i>	<i>kap4 -/-</i>
2S2N1K	1,5%	0,0%	1,6%
1S2N1K	0,0%	1,7%	3,1%
1S2NOK	0,0%	0,0%	0,8%
1Fs1N1K	3,7%	0,0%	0,0%
1Fs1NOK	0,7%	0,0%	0,0%
OS1N1K	0,7%	2,9%	2,3%
Fragmented DNA	3,0%	1,1%	1,6%

## Cisplatin treatment

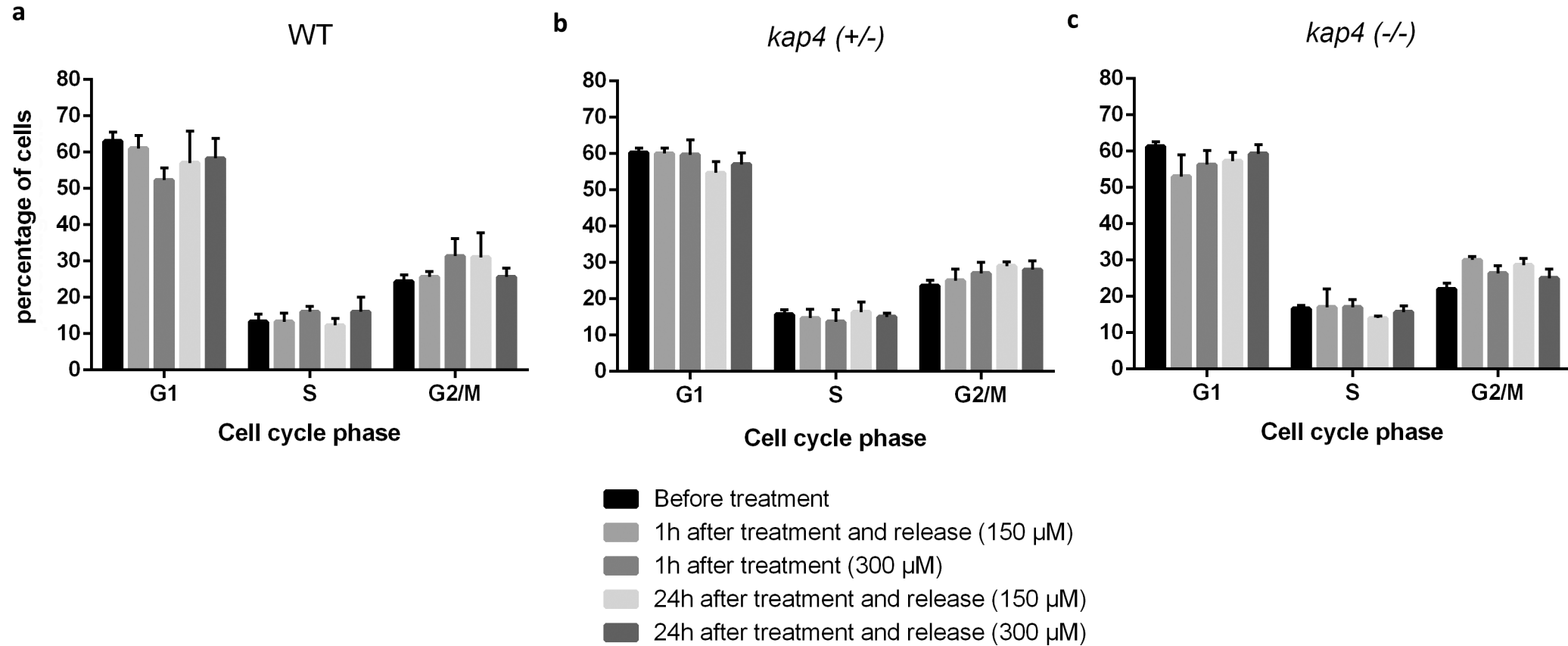


## Ultraviolet radiation





**Supplementary Material 1:** Total protein extract of WT and T7RNAPol-SpCas9 mutant strains of *A. deanei* and *L. mexicana*, here used as a control, were probed with anti-FLAG antibody (Anti-FLAG M2, Sigma F3165; dilution 1:20,000) for detection of SpCas9 or anti- $\beta$ -tubulin (Anti- $\beta$ -Tubulin clone AA2, Sigma T8328; dilution 1:10,000) used as loading control.



**Supplementary Material 2:** Flow cytometry analysis of *A. deanei* DNA content in wild type (WT) and mutant cells treated or not with cisplatin for 1 h or 24 h.

<b>Wild type</b>	<b>Replicate 1</b>		<b>Replicate 2</b>	
<b>Small blank</b>	1456	1121	1205	1190
<b>Small NT</b>	29656	28775	29332	29011
<b>Small 0,25h</b>	28744	28312	31223	30774
<b>Small 1h</b>	28552	28331	30999	31421
<b>Small 3h</b>	27561	28078	30657	30212
<b>Small 6h</b>	27771	26987	29044	27908
<b>Kap4+/-</b>	<b>Replicate 1</b>		<b>Replicate 2</b>	
<b>Small blank</b>	1987	1999	1024	1016
<b>Small NT</b>	30999	31647	32886	32543
<b>Small 0,25h</b>	29767	29342	31888	31369
<b>Small 1h</b>	30145	29987	29042	29466
<b>Small 3h</b>	29688	28921	33112	33876
<b>Small 6h</b>	27556	27899	29234	30450
<b>Kap4-/-</b>	<b>Replicate 1</b>		<b>Replicate 2</b>	
<b>Small blank</b>	1113	997	1002	996
<b>Small NT</b>	26684	27499	29500	29122
<b>Small 0,25h</b>	27312	27484	28666	27521
<b>Small 1h</b>	25433	26421	29311	29875
<b>Small 3h</b>	26911	26041	26884	28333
<b>Small 6</b>	25987	26020	26003	27421

**Supplementary Material 3:** DNA repair kinetics (0.25-6 h) measured by long-range qPCR. Absorbance values for the smaller fragments of *A. deanei* WT, kap4+/- and kap4-/-.